The interaction of resonant magnetic perturbations with rotating plasmas

R. Fitzpatrick and T. C. Hender

Articles you may be interested in

Continuum resonance induced electromagnetic torque by a rotating plasma response to static resonant magnetic perturbation field
Phys. Plasmas **19**, 102507 (2012); 10.1063/1.4759205

Gyrokinetic simulations with external resonant magnetic perturbations: Island torque and nonambipolar transport with plasma rotation
Phys. Plasmas **19**, 032508 (2012); 10.1063/1.3692222

Shielding of resonant magnetic perturbations by rotation
Phys. Plasmas **3**, 4620 (1996); 10.1063/1.871585

Interaction between resonant magnetic perturbation and the rotating magnetic island
Phys. Plasmas **1**, 946 (1994); 10.1063/1.870753

Plasma Resonance Interaction with a Spatially Rotating Static Magnetic Field
Phys. Fluids **6**, 501 (1963); 10.1063/1.1706764

The interaction of resonant magnetic perturbations with rotating plasmas

R. Fitzpatrick and T. C. Hender
Culham Laboratory (Euratom/UKAEA Fusion Association), Abingdon, OX14 3DB, England

The penetration of a helical magnetic perturbation into a rotating tokamak plasma is investigated. In the linear regime, it is found that unless the frequency of the imposed perturbation matches closely to one of the natural mode frequencies, reconnection at the rational surface is suppressed by a large factor. In order to deal with the problem in the nonlinear regime a theory of propagating, constant-ψ magnetic islands is developed. This theory is valid provided the island width greatly exceeds any microscopic scale length (but still remains small compared with the minor radius), and the magnetic Reynolds number of the plasma is sufficiently large. An island width evolution equation is obtained which, in addition to the usual Rutherford term, contains a *stabilizing* term due ultimately to the inertia of the plasma flow pattern set up around the propagating island. A complete solution is presented for the case where the island and its associated flow pattern are steady. In the nonlinear regime, a fairly sharp threshold is predicted for the magnitude of the applied perturbation. Below this threshold, the induced islands are rotationally suppressed and partially dragged along by the rotating plasma, and above it the islands are virtually fully reconnected and "locked" at the applied frequency of the perturbation. Numerical results from an initial value code are presented, which show good agreement with the analytic predictions. Finally, it is demonstrated that these theories can be used to interpret data recently obtained from the COMPASS-C device [*Controlled Fusion and Plasma Heating 1990* (EPS, Geneva, 1990), Vol. 1, p. 379]. In particular, a possible explanation is given of why in some cases an applied quasistatic resonant magnetic perturbation can stabilize magnetohydrodynamic modes, but in others leads to a disruption.

I. INTRODUCTION

In this paper we shall investigate what happens when a resonant (m, n) magnetic perturbation, with a given frequency Ω, is applied to a tokamak plasma whose natural (m, n) mode frequency is significantly different to Ω. Here, m is the poloidal mode number and n the toroidal mode number. There are three main types of experimental situation that are pertinent to this investigation:

(1) In several tokamak experiments resonant magnetic perturbations have been deliberately applied using coils external to the plasma (for instance, PULSATOR,[1] TOSCA,[2] and recently COMPASS-C[3]). Such perturbations are used to control and influence the internal magnetohydrodynamic (MHD) activity. Generally speaking this activity has a finite frequency, due to the combined effects of diamagnetic and $E \wedge B$ drifts, whilst the applied perturbations are either stationary or rotate at a much lower frequencies than those of the natural modes.[1-3]

(2) The slight misalignment of the magnetic field coils that must inevitably occur in all tokamaks gives rise to a so-called "error field," which has small (but non-negligible) components resonant on all low mode-number rational surfaces in the plasma. Error fields are generally thought to be responsible for the ultimate mode locking of large magnetic islands that is often observed in experiments.[4] Error fields are also thought to induce small permanent magnetic islands on all low mode-number rational surfaces. If these islands are wider than a typical linear layer width, as a naive calculation with no rotation effects would tend to indicate, then it is

difficult to see how the results of linear layer theory could ever be applicable to experiments. Rotation effects are likely to be important in this situation, because error fields are static, whereas the plasma generally rotates under the influence of diamagnetic and $E \wedge B$ drifts.

(3) The toroidal eigenmode for an (m, n) tearing mode contains poloidal harmonics whose principle components are resonant on the $(m \pm 1, n)$ rational surfaces.[5] Thus, the presence of an island on the (m, n) rational surface gives rise, via toroidal coupling, to small magnetic perturbations resonant on neighboring rational surfaces. Naturally, these applied perturbations will rotate at the frequency of the (m, n) mode, which in general will be significantly different to those of the natural $(m \pm 1, n)$ modes. (See Ref. 6 for a description of a simple linear theory of this phenomenon.) Toroidal coupling is interesting because it gives rise to modes that simultaneously reconnect magnetic flux at more than one rational surface.

In this paper we shall restrict ourselves to cylindrical geometry, which is a perfectly adequate framework for an analysis of the first two situations described above. Clearly, we cannot hope to deal with the third situation in such a geometry. We note, however, that the layer theory presented in Secs. II and III, together with the coupling theory of Ref. 5 for the "outer" ideal magnetohydrodynamic (MHD) solution, would provide a suitable framework to treat the toroidal coupling problem.

We shall consider the interaction of resonant magnetic perturbations and rotating plasmas in both the linear and nonlinear regimes. Obviously, our linear results have only a

very limited application to experiments. However, they have the advantage of being relatively clear-cut and, furthermore, provide a useful point of reference for the interpretation of our nonlinear results.

We shall mainly concentrate on the situation where the natural (m, n) plasma mode is *stable*, and so any reconnection that occurs at the (m, n) rational surface is entirely due to the externally applied magnetic perturbation. We call this situation *"forced reconnection"*. Clearly, it would not be sensible to consider the case of a naturally unstable (m, n) mode in the linear regime, because of the absence of any effective saturation mechanism. In the nonlinear regime, however, it is possible to envisage a situation where the externally applied resonant perturbation interacts with a *pre-existing* saturated magnetic island. Our nonlinear results are also applicable to this case, once the saturation mechanism (i.e., the quasilinear modification to the external Δ' due to finite island size)[7] is taken into account.

We shall tackle the problem of the interaction of rotating plasmas with applied helical perturbations using both analytic and numerical techniques. In the next two sections the analytic results are derived, and then in Sec. IV simulations using an initial-value code are presented. The analytic results will be shown to be in good agreement with the numerical simulations, and provide physics insight into the observed behavior.

II. LINEAR THEORY OF FORCED RECONNECTION IN ROTATING PLASMAS

A. Introduction

The analysis used in this section is a direct extension of that employed by Hahm and Kulsrud,[8] who considered the linear theory of forced reconnection in a *nonrotating* plasma.

Consider a cylindrical plasma equilibrium of radius a and effective major radius R. We refer to this equilibrium using a standard right-handed set of cylindrical polar coordinates (r, θ, z), and define a effective toroidal angle $\zeta = z/2\pi R$. The perturbed magnetic field is written

$$\mathbf{B}_1 = \nabla\psi \wedge \hat{\mathbf{z}}, \tag{1}$$

where $\psi(r, \theta, \zeta)$ is the perturbed magnetic flux. For an (m, n) mode resonant at $r = r_s$ inside the plasma, $\psi(r, \theta, \zeta)$ takes the form

$$\psi(r)e^{i(m\theta - n\zeta)}. \tag{2}$$

Throughout the ideal MHD region the perturbed flux satisfies

$$L_{(m,n)}\psi(r) = 0, \tag{3}$$

where $L_{(m,n)}$ is the cylindrical Euler–Lagrange operator obtained by minimizing the ideal MHD quantity δW for an (m, n) mode.[5] Appropriate boundary conditions are that $\psi(r)$ is regular at $r = 0$, and $\psi(a) = 0$. The latter condition corresponds to the presence of a conducting wall at the edge of the plasma. Of course, more physically realistic boundary conditions, including effects such as vacuum regions immediately outside the plasma and resistive walls,[9] could be specified at this stage. We have chosen a close-fitting conducting wall merely to simplify the analysis.

In general, the solution to Eq. (3) that satisfies the appropriate boundary conditions (referred to henceforth as ψ_0) has a gradient discontinuity at the rational surface $r = r_s$, indicating the presence of an effective current sheet there. The magnitude of this current sheet is parametrized by

$$\Delta_0' = \left(\frac{\partial\psi_0}{\partial r}\right)^{r_{s+}}_{r_{s-}} [\psi_0(r_s)]^{-1} \tag{4}$$

which is also a measure of the amount of free-energy available to drive a reconnecting mode.[10]

The gradient discontinuity in the ideal solution is resolved by resistivity, which only becomes important in a thin layer centered on the rational surface. After solving for $\psi(r)$ across the resistive layer it is possible to construct a quantity Δ (basically, the ratio of the coefficients of the two power-law asymptotic forms at the edge of the layer)[11] that must be set equal to Δ_0' in order that the layer solution match correctly onto the outer ideal MHD solution. In the linear regime, where perturbed layer quantities are assumed to have an $e^{-i\omega t}$ time dependence, Δ is just a function of ω and local equilibrium quantities.

B. The time-asymptotic steady-state solution

Suppose that the plasma boundary is subject to some externally applied perturbation such that the modified boundary lies at

$$r = a + \delta e^{i(m\theta - n\zeta)}e^{-i\Omega t}. \tag{5}$$

It is assumed throughout this paper that Ω, the oscillation frequency of the applied perturbation, is much less than the Alfvén transit frequency across the plasma, so that the outer ideal MHD solution is always in equilibrium with the boundary. It is further assumed that $\delta \ll a$, so that the outer solution is *linear* (we assume that this condition is satisfied even in the so-called "nonlinear" regime discussed later on in this paper). The modified boundary condition applicable at $r = a$ is

$$\psi(a) = [(\mathbf{k}\cdot\mathbf{B}_0)/k_\theta]\delta e^{-i\Omega t}. \tag{6}$$

Here, $\mathbf{k} \equiv (0, m/r, -n/R)$ is the wave vector of the perturbation and $\mathbf{B}_0$ is the equilibrium magnetic field. A suitable solution to Eq. (3), which satisfies the boundary condition (6), can be constructed as follows:

$$\psi(r, t) = \Psi(t)\hat{\psi}_0(r) + \psi_1(r)e^{-i\Omega t}. \tag{7}$$

Here, $\hat{\psi}_0(r) = \psi_0(r)/\psi_0(r_s)$, while $\Psi(t)$ represents the amount of reconnected flux at the rational surface. The function $\psi_1(r)$ is a solution of (3), which is zero for $r \leqslant r_s$, and satisfies the boundary condition $\psi_1 = [(\mathbf{k}\cdot\mathbf{B}_0)/k_\theta]\delta$ at $r = a$. The two contributions to $\psi(r)$ are shown schematically in Fig. 1.

Equation (7) implies that the modified Δ' has the form

$$\Delta' = \Delta_0' + [\psi_1'(r_s)/\Psi(t)]e^{-i\Omega t}. \tag{8}$$

Recall, that to obtain the correct matching between the inner solution and the outer solution Δ' must be set equal to the quantity $\Delta(\omega)$ calculated from the layer. If, in addition, we wish to obtain a final steady state, it is necessary that $\Psi(t) = \Psi e^{-i\Omega t}$ (i.e., $\omega = \Omega$), where Ψ is a constant. Thus, in the linear regime, Eq. (8) yields
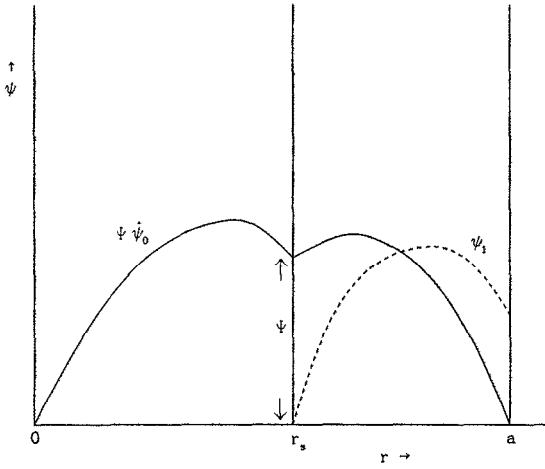
FIG. 1. A schematic diagram showing the two contributions to $\psi(r)$ at $t = 0$ [cf. Eq. (7)]. The function $\hat{\psi}_0(r)$ is the normalized unperturbed (m, n) radial eigenfunction; its gradient discontinuity at the rational surface, $r = r_s$, is parametrized by the quantity Δ_0'. The quantity Ψ represents the amount of reconnected flux at the rational surface. The function $\psi_1(r)$ is driven by the applied perturbation at the edge of the plasma, $r = a$.

$$\Psi/\Psi_c = [1 + \Delta(\Omega)/(-\Delta_0')]^{-1} \qquad (9)$$

as the time-asymptotic solution. Here,

$$\Psi_c = \psi_1'(r_s)/(-\Delta_0') \qquad (10)$$

is the amount of reconnected flux driven by the applied perturbation in the absence of any current sheet at the rational surface.

C. The dynamic solution

Consider now the dynamic response of a layer to a perturbation of the boundary $\delta e^{i(m\theta - n\varsigma)}e^{-i\Omega t}$ applied at $t = 0$. Let

$$\tilde{\psi}(r,s) = \int_0^\infty dt\, e^{-st}\psi(r,t). \qquad (11)$$

Equations (7) and (11) yield

$$\tilde{\psi}(r,s) = \tilde{\Psi}(s)\hat{\psi}_0(r) + \psi_1(r)/(s + i\Omega). \qquad (12)$$

Equation (12) implies that

$$\Delta' = \Delta_0' + [\psi_1'(r_s)/\tilde{\Psi}(s)]/(s + i\Omega). \qquad (13)$$

Now, in the linear regime, the Laplace transformed resistive layer equations have exactly the same form as the equations derived using an $e^{-i\omega t}$ time dependence, provided that $\Psi(t = 0) = 0$ and with the quantity is substituted for ω. Clearly, in order to properly match the layer and the outer ideal MHD solutions, Δ' in Eq. (13) must be set equal to $\Delta(is)$. Thus, Eq. (13) yields

$$\frac{\Psi(t)}{\Psi_c(t)} = \frac{1}{2\pi i}\int_{\mathscr{C}} \frac{ds\, e^{(s + i\Omega)t}}{[1 + \Delta(is)/(-\Delta_0')]} \frac{1}{(s + i\Omega)}, \qquad (14)$$

where $\Psi_c(t) = \Psi_c e^{-i\Omega t}$ and $\mathscr{C}$ is the Bromwich contour. Provided that all of the roots of $\Delta(is) = \Delta_0'$ lie on the left-hand side of the s plane [i.e., provided that the (m, n) mode

is intrinsically stable] the $t \to \infty$ limit of (14) is in agreement with Eq. (9).

D. The solution in the collisional regime

The derivation of the formulas (9) and (14) is completely independent of the nature of the resistive layer. However, in order to obtain any useful information from these formulas it is now necessary to assume a definite form for the layer solution. In this subsection, as an illustrative example, we consider the collisional layer dynamics of Ara et al.,[12] corresponding to the simplest possible choice of layer physics that takes into account diamagnetic and $E \wedge B$ drifts.

1. The collisional dispersion relation

It is demonstrated in Ref. 12 that the dispersion relation for a constant-ψ, drift-tearing mode, derivable from a set of collisional layer equations in slab geometry, takes the form

$$(\Delta r_s) = 2\pi[\Gamma(3/4)/\Gamma(1/4)]\mu^{1/4}(\mu + i\mu_e)^{3/4}$$
$$\times (\mu + i\mu_i)^{1/4}, \qquad (15)$$

where

$$\mu = -i\omega'\tau_c, \quad \mu_e = \omega_{*e}\tau_c, \quad \mu_i = \omega_{*i}\tau_c. \qquad (16)$$

(See Refs. 10 and 13 for definitions of the terms "constant ψ" and "collisional".) Here, $\omega' = \omega - k_\theta u_{eq}$, where u_{eq} is the $E \wedge B$ velocity of the unperturbed plasma at the rational surface. In (16), ω_{*e} is the local electron diamagnetic frequency, ω_{*i} the local ion diamagnetic frequency, and $\tau_c = S^{3/5}\tau_H$ the typical reconnection time-scale of a drift-tearing mode. The quantity S is the local magnetic Reynolds number, while τ_H is the local hydromagnetic time scale, and Γ is a standard gamma function. (All of these quantities are fully defined in Ref. 12.) Note that Eq. (15) is only valid in the limit where the ion Larmor radius is much less than the resistive layer width. The constant-ψ approximation holds provided that all frequencies in the local $E \wedge B$ frame (i.e., Ω', ω', ω_{*e}, etc.) lie well below τ_E^{-1}, where $\tau_E = S^{1/3}\tau_H$ is the typical lifetime of a resistively damped ideal eddy and, consequently, the typical time scale associated with a resistive internal kink mode.

In general, the expression (15) is multivalued. However, any ambiguity is removed by the requirement that all cuts lie in the left-hand side of the μ plane. (If this were not the case the Fourier transform solution would not be the time-asymptotic limit of the Laplace transform solution.) Another requirement is that $\arg(\Delta) \to 0$ when μ is real, positive, and much greater in magnitude than $|\mu_e|$ and $|\mu_i|$.

2. The collisional time-asymptotic steady-state solution

In the constant-ψ, collisional regime, the final amount of reconnection induced by an imposed perturbation of frequency Ω is calculated by substituting the dispersion relation (15) (with $\omega = \Omega$) into Eq. (9). Note that for collisional layer dynamics, the requirement that the (m, n) mode be intrinsically stable implies a negative Δ_0'.

The final amount of reconnected flux, calculated in the manner described above, in the limit where the diamagnetic frequencies ω_{*e} and ω_{*i} are both negligible, is given by

$$\Psi/\Psi_c = 1/(1 + e^{-i5\pi/8}\lambda\mu_c^{5/4}), \qquad (17)$$

where

$$\mu_c = \Omega'\tau_c. \qquad (18)$$

Here,

$$\lambda = [2\pi/(-\Delta_0'r_s)][\Gamma(3/4)/\Gamma(1/4)], \qquad (19)$$

while

$$\Omega' = \Omega - k_\theta u_{eq} \qquad (20)$$

is the Doppler-shifted oscillation frequency of the applied perturbation as seen in a frame moving with the local equilibrium $\mathbf{E} \wedge \mathbf{B}$ velocity at the rational surface. Figure 2 shows the magnitude and phase of Ψ/Ψ_c, calculated in accordance with Eq. (17), for $\lambda = 1$. It can be seen that if the Doppler-shifted perturbation frequency is significantly greater than the linear damping rate of the unforced reconnecting mode, $|\gamma_0| \sim \lambda^{-4/5}/\tau_c$, then the final amount of reconnection is much less than that obtained in the absence of any rotation. Furthermore, a substantial phase shift is introduced between the induced perturbation at the rational surface and the applied perturbation on the boundary. Note that a small amount of rotation actually enhances reconnection slightly. The strong resonance at $\Omega' = 0$ occurs because at this frequency the applied magnetic perturbation moves with the local equilibrium fluid velocity at the rational surface.

The final amount of reconnection obtained when the diamagnetic frequencies are non-negligible is given by

$$\frac{\Psi}{\Psi_c} = \frac{1}{[1 + e^{-i5\pi/8}\lambda\mu_c^{1/4}(\mu_c - \mu_e)^{3/4}(\mu_c - \mu_i)^{1/4}]}. \qquad (21)$$

Figure 3 shows the magnitude and phase of Ψ/Ψ_c, calculated in accordance with the above formula for the case where the typical diamagnetic frequencies are significantly greater than the reconnection rate (i.e., $|\mu_e|, |\mu_i| \gg 1$). It can be seen that there are now three very sharp resonances, at $\Omega' = \omega_{*e}$, 0, and ω_{*i}, respectively. The widths of these resonances are of order the typical linear damping rates $[|\gamma_e| \sim \omega_*/Q^{4/3}, |\gamma_g| \sim |\gamma_i| \sim \omega_*/Q^4$, cf. (22)] of the unforced electron, low-frequency, and ion modes, respectively. In between the resonances, the amount of reconnection falls to a value of order $1/Q$, where

$$Q \sim \lambda[\omega_*\tau_c]^{5/4}. \qquad (22)$$

In the above, ω_* is a typical diamagnetic frequency. In fact, a collisional resistive layer acts very much like a tuned oscillator, with a typical "Q-factor" (basically, a measure of the frequency selectivity) given by Eq. (22). Note that the electron resonance is significantly wider than the other two resonances. The resonance at $\Omega' = \omega_{*i}$ occurs because at this frequency the applied magnetic perturbation moves with the local velocity of the ion fluid at $r = r_s$. Similarly, at $\Omega' = \omega_{*e}$ the perturbation moves with the local electron fluid velocity, and at $\Omega' = 0$ the perturbation moves with the local velocity of the particle guiding centers.

It is fairly clear from the above calculations that an externally applied (m, n) magnetic perturbation is only likely to induce a significant amount of reconnection at the mode rational surface if its frequency, Ω, is close to one of the
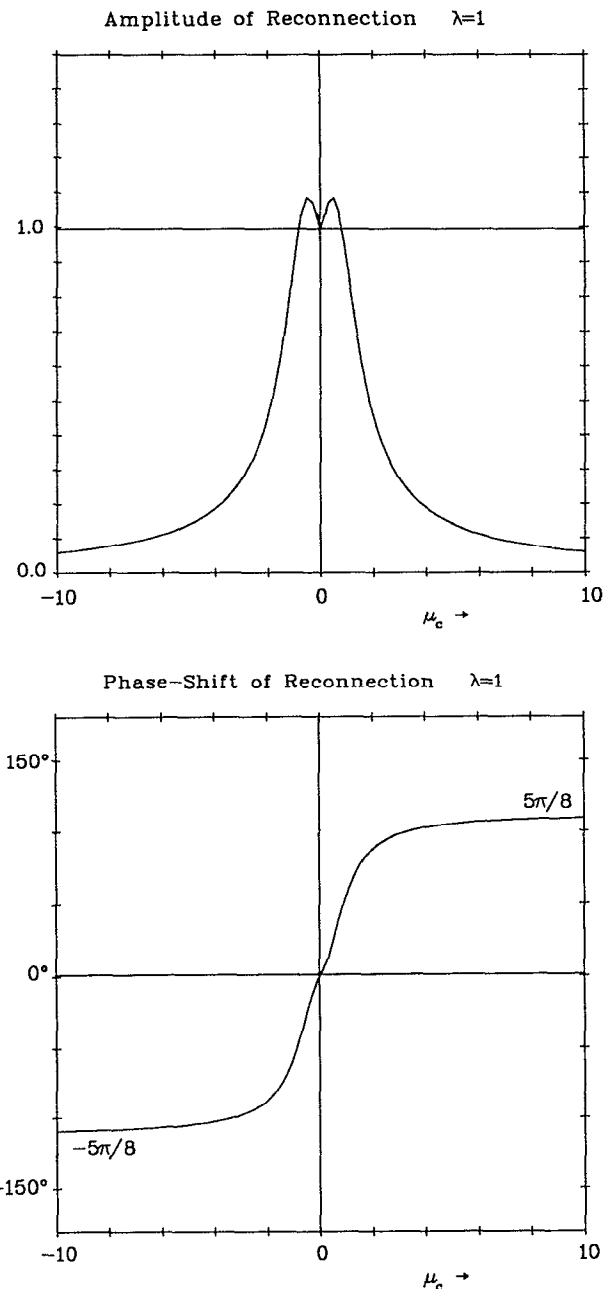

Amplitude of Reconnection $\lambda = 1$

Phase-Shift of Reconnection $\lambda = 1$

FIG. 2. The final amplitude (i.e., $|\Psi/\Psi_c|$) and phase (i.e., $\arg\{\Psi/\Psi_c\}$) of reconnection induced by a resonant magnetic perturbation, of frequency Ω, applied at the edge of a *nondiamagnetic* plasma. The quantity $\mu_c = \Omega'\tau_c$, where $\tau_c = S^{3/5}\tau_H$, measures the relative rotation frequency of the plasma at the rational surface with respect to the applied signal. In the above diagram $\lambda = 1$ [cf. Eq. (19)]. The amplitude of reconnection is strongly peaked at $\Omega' = 0$, with a typical width (in Ω') $|\gamma_0| \sim \lambda^{-4/5}/\tau_c$, where γ_0 is the linear damping rate of the unforced reconnecting mode.

unforced oscillation frequencies of the (m, n) mode—the typical width of any resonance is always of order the unforced linear damping rate.

3. The collisional dynamic solution

The dynamic response of a constant-ψ, collisional layer to an external magnetic perturbation applied suddenly at

Amplitude of Reconnection $\lambda=1$
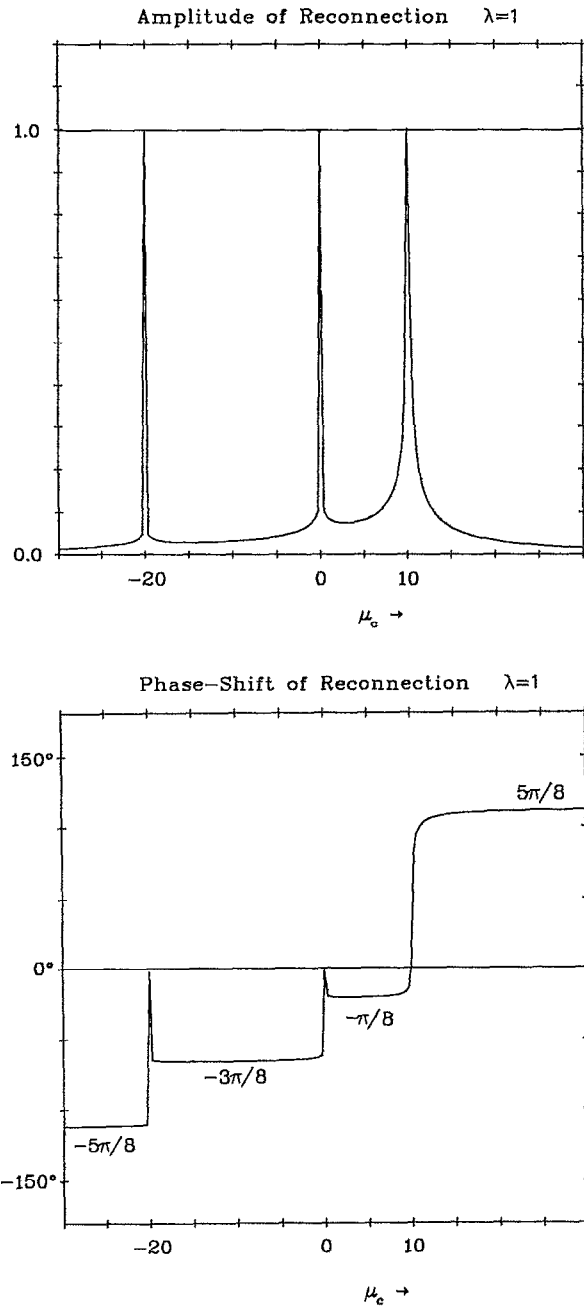

Phase-Shift of Reconnection $\lambda=1$

FIG. 3. The final amplitude (i.e., $|\Psi/\Psi_c|$) and phase (i.e., $\arg\{\Psi/\Psi_c\}$) of reconnection induced by a resonant magnetic perturbation, of frequency Ω, applied at the edge of a *diamagnetic* plasma. In the above diagrams $\lambda = 1$, $\mu_c = \omega_{*e}\tau_c = 10$, and $\mu_i = \omega_{*i}\tau_c = -20$. The amplitude of reconnection is strongly peaked at $\Omega' = \omega_{*e}$, 0, and ω_{*i}, respectively. Note that for this case $Q \sim 30$ [cf. Eq. (22)].

$t = 0$ can be calculated by substituting the dispersion relation (15) (with $\omega = is$) into Eq. (14).

If the diamagnetic frequencies are negligible, we obtain

$$\frac{\Psi(\tau)}{\Psi_c(\tau)} = \frac{1}{2\pi i} \int_c \frac{dp\, e^{(p+i\mu_c)\tau}}{(1+\lambda p^{5/4})} \frac{1}{(p+i\mu_c)}, \qquad (23)$$

where

$$\tau = t/\tau_c. \qquad (24)$$

The contour integral in Eq. (23) can be decomposed into elements from the three poles (at $p_c = -i\mu_c$, and $p_\pm = e^{\pm i4\pi/5}\lambda^{-4/5}$, respectively) plus a contribution from the cut along the $p = e^{i\pi}u$ axis (where u is real and positive), giving

$$\frac{\Psi(\tau)}{\Psi_c(\tau)} = \frac{1}{[1+e^{-i5\pi/8}\lambda\mu_c^{5/4}]}$$

$$- \frac{4}{5}\left(\frac{p_+ e^{(p_+ +i\mu_c)\tau}}{(p_+ +i\mu_c)} + \frac{p_- e^{(p_- +i\mu_c)\tau}}{(p_- +i\mu_c)}\right)$$

$$+ \frac{\lambda}{\sqrt{2}\pi}\int_0^\infty \frac{du\, u^{5/4}e^{-(u-i\mu_c)\tau}}{(1-\sqrt{2}\lambda u^{5/4}+\lambda^2 u^{5/2})}$$

$$\times \frac{1}{(u-i\mu_c)}. \qquad (25)$$

Figure 4 shows the amplitude and phase of $\Psi(\tau)/\Psi_c(\tau)$, evaluated numerically from the above expression, for $\mu_c = 0$, 5, and 50, with $\lambda = 1$. For the "resonant" (in relative frequency) case, $\mu_c = 0$, expression (25) can be evaluated analytically in certain limits, giving

$$\frac{\Psi(t)}{\Psi_c(t)} \simeq \frac{8\sqrt{2}}{5\pi}\Gamma\left(\frac{3}{4}\right)\left(\frac{t}{\tau_0}\right)^{5/4}, \quad t\ll\tau_0,$$

$$\frac{\Psi(t)}{\Psi_c(t)} \simeq 1 - \frac{\Gamma(5/4)}{\sqrt{2}\pi}\left(\frac{\tau_0}{t}\right)^{5/4}, \quad t\gg\tau_0. \qquad (26)$$

Figure 4 and Eq. (26) imply that if a "resonant" (i.e., $\mu_c = 0$) perturbation is applied to the plasma at $t = 0$, then the reconnection induced at the rational surface will increase rapidly on a time scale $\tau_0 = \lambda^{4/5}\tau_c$, overshoot slightly, and settle down to an amount given by Eq. (17). [N.B. This result and expression (26) were first derived in Ref. 8, and are only described here for the sake of comparison.] Note that there is always zero phase shift between the perturbation at $r = r_s$, and the imposed perturbation at the plasma edge. Note, also, that $\tau_0 = 1/|\gamma_0|$, where γ_0 is the linear damping rate of the unforced reconnecting mode. Figure 4 also shows that if a strongly "nonresonant" (i.e., $|\mu_c|\gg1$) perturbation is applied to the plasma at $t = 0$, then the amount of reconnection induced at the rational surface performs relatively large amplitude oscillations at the imposed frequency, before settling down to some final value on a time-scale which is again τ_0. Note that the final amount of reconnection [again given by Eq. (17)] is always significantly less than that obtained from a completely "resonant" perturbation. Note, further, that in the "nonresonant" case a significant phase shift is set up, on a time scale τ_0, between the perturbation at the rational surface and the imposed perturbation at the edge.

When the diamagnetic frequencies are non-negligible, Eqs. (14) and (15) yield

$$\frac{\Psi(\tau)}{\Psi_c(\tau)} = \frac{1}{2\pi i}$$

$$\times \int_c \frac{dp\, e^{(p+i\mu_c)\tau}}{[1+\lambda p^{1/4}(p+i\mu_e)^{3/4}(p+i\mu_i)^{1/4}](p+i\mu_c)}. \qquad (27)$$
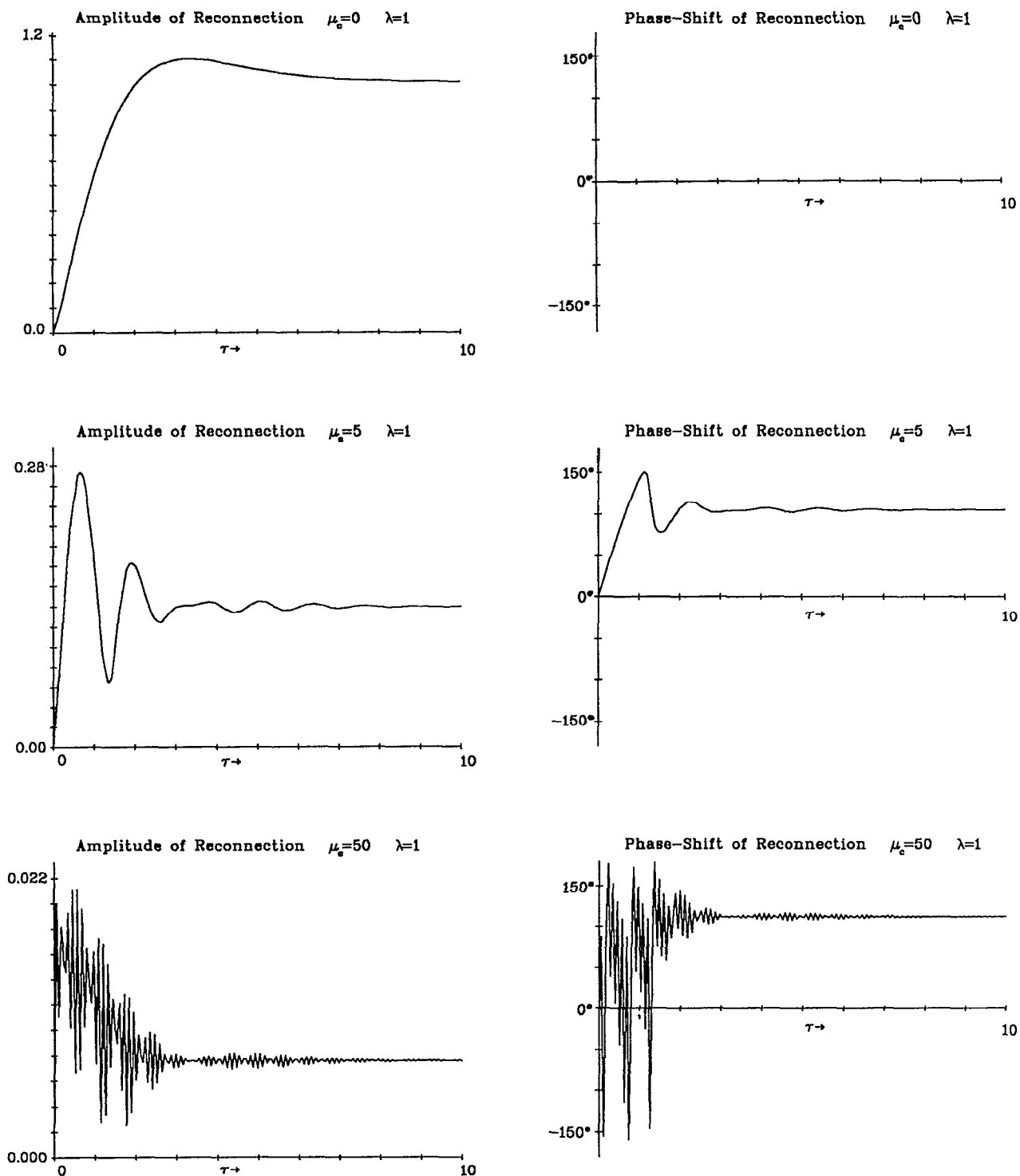
FIG. 4. The amplitude (i.e., $|\Psi/\Psi_c|$) and phase (i.e., $\arg\{\Psi/\Psi_c\}$) of reconnection induced by a resonant magnetic perturbation of frequency Ω, applied at the edge of a *nondiamagnetic* plasma at $t = 0$. The quantity $\tau = t/\tau_c$ is the normalized time. Note that the typical time required to achieve a final steady state (i.e., $\tau_0 = \lambda^{4/5}\tau_c$) is virtually independent of the relative rotation of the plasma.

Figure 5 shows the amplitude of $\Psi(\tau)/\Psi_c(\tau)$, evaluated numerically from the above expression, for various values of μ_c, with $\mu_e = 5$, $\mu_i = -5$, and $\lambda = 4$. For the three "resonant" cases ($\mu_c = \mu_i$, 0, and μ_e, respectively) the dominant (i.e., nonoscillating) contributions to the expression (27) can be evaluated analytically in certain limits. Thus, for the ion resonance we obtain

$$\frac{\Psi(t)}{\Psi_c(t)} \simeq e^{-i\pi/2}\frac{2\sqrt{2}}{\pi}\,\Gamma\!\left(\frac{3}{4}\right)\!\left(\frac{t}{\tau_i}\right)^{1/4}, \quad t \ll \tau_i,$$

$$\frac{\Psi(t)}{\Psi_c(t)} \simeq 1 - e^{i\pi/2}\frac{\Gamma(1/4)}{\sqrt{2\pi}}\left(\frac{\tau_i}{t}\right)^{1/4}, \quad t \gg \tau_i, \qquad (28)$$
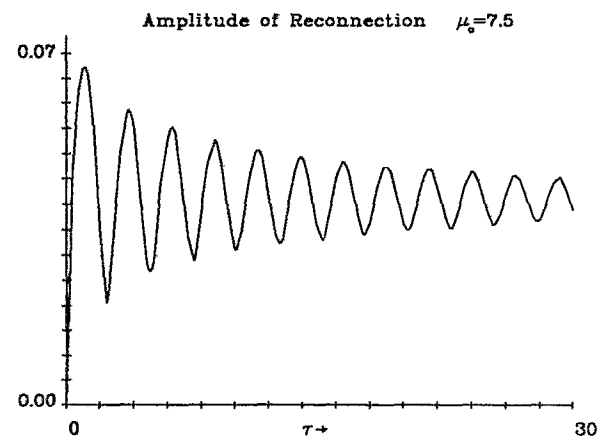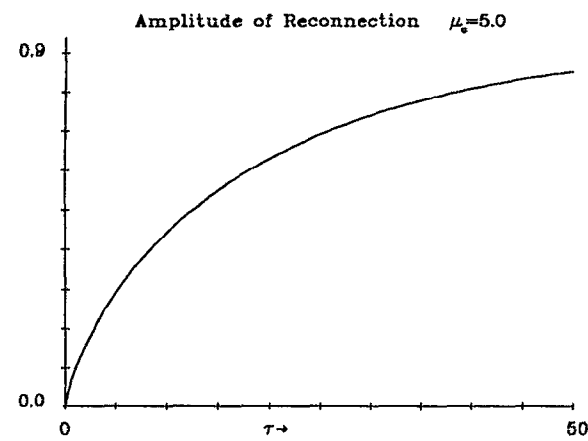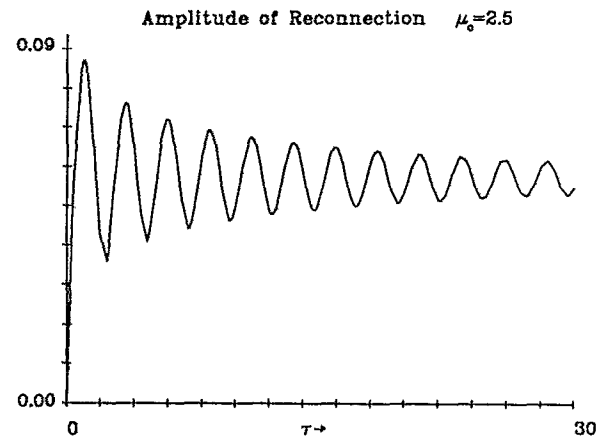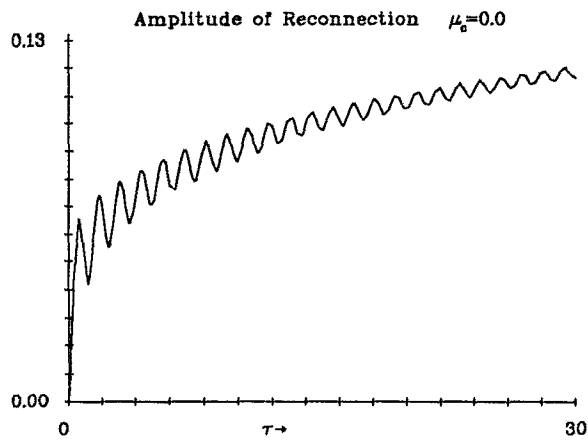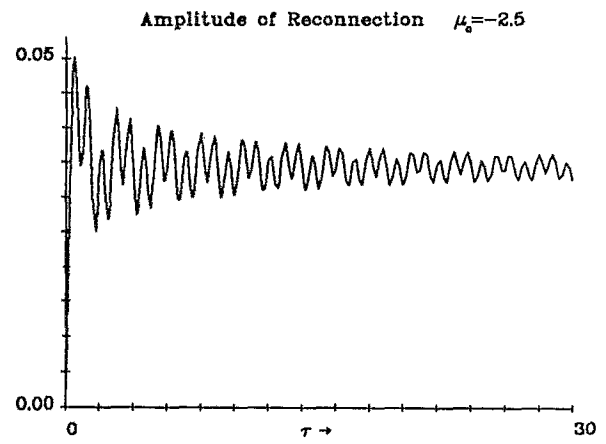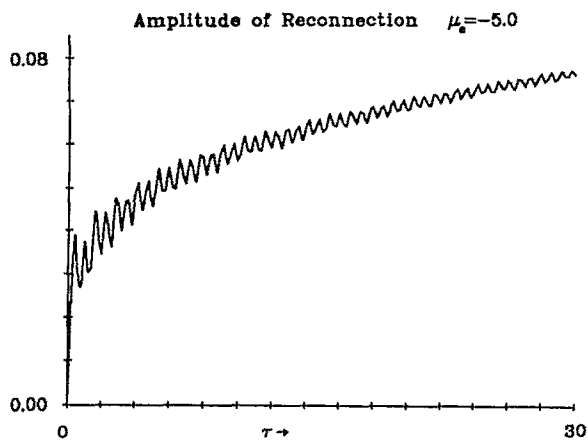
with

FIG. 5. The amplitude (i.e., $|\Psi/\Psi_c|$) of reconnection induced by a resonant magnetic perturbation, of frequency Ω, applied to the edge of a *diamagnetic* plasma at $t = 0$. The quantity $\tau = t/\tau_c$ is the normalized time. In the above diagrams $\lambda = 4$, $\mu_c = \omega_{*c}\tau_c = 5$, and $\mu_i = \omega_{*i}\tau_c = -5$.

$$\frac{\Psi(t)}{\Psi_c(t)} \simeq e^{-i\pi/4}\frac{2\sqrt{2}}{\pi}\,\Gamma\!\left(\frac{3}{4}\right)\!\left(\frac{t}{\tau_g}\right)^{1/4}, \quad t \ll \tau_g,$$

$$\frac{\Psi(t)}{\Psi_c(t)} \simeq 1 - e^{i\pi/4}\frac{\Gamma(1/4)}{\sqrt{2\pi}}\left(\frac{\tau_g}{t}\right)^{1/4}, \quad t \gg \tau_g, \qquad (29)$$

for the small-frequency resonance, and

$$\frac{\Psi(t)}{\Psi_c(t)} \simeq e^{i\pi/4}\frac{4}{3\sqrt{2\pi}}\left(\frac{t}{\tau_e}\right)^{3/4}, \quad t \ll \tau_e,$$

$$\frac{\Psi(t)}{\Psi_c(t)} \simeq 1 - e^{-i\pi/4}\frac{\Gamma(3/4)}{\sqrt{2\pi}}\left(\frac{\tau_e}{t}\right)^{3/4}, \quad t \gg \tau_e, \qquad (30)$$

for the electron resonance. The various reconnection rates in

the above expressions are given by

$$\tau_i = \lambda^4 \mu_i (\mu_i + \mu_e)^3 \tau_c \equiv 1/|\gamma_i|,$$
$$\tau_g = \lambda^4 \mu_i \mu_e^3 \tau_c \equiv 1/|\gamma_g|, \qquad (31)$$
$$\tau_e = \lambda^{4/3} \mu_e^{1/3} (\mu_i + \mu_e)^{1/3} \tau_c \equiv 1/|\gamma_e|,$$

where γ_i, γ_g, and γ_e are the linear damping rates of the unforced ion, low-frequency, and electron modes, respectively. Note that if $|\mu_i|$, $|\mu_e| \gg 1$, then the rate of reconnection is slowed down considerably at the electron resonance. At the ion and low-frequency resonances, however, the rate of reconnection is slowed down so drastically that it is unlikely that the system can ever attain full reconnection (i.e., $\Psi = \Psi_c$) under realistic conditions. The results presented in Fig. 5 show good agreement with Eqs. (28)–(31), and are also consistent with the expression (21) in the time-asymptotic limit.

The effects of bulk plasma rotation and diamagnetic rotation can now be compared and contrasted. Bulk plasma rotation acts so as to Doppler shift the natural mode frequencies of the resistive layer, thereby reducing the amount of reconnection induced by a (for the sake of argument) static externally applied magnetic perturbation, but it does not modify the rate at which such reconnection proceeds. Substantial diamagnetic flows, on the other hand, not only modify the resonant frequencies of the resistive layer, again reducing the reconnection induced by an external static perturbation, they also greatly (in some cases drastically) reduce the rate to which such reconnection proceeds.

E. Discussion

For Ohmically heated plasmas in modern tokamaks, the typical equilibrium toroidal rotation frequency ($f_{rot} \sim k_\theta u_{eq}/2\pi$) is generally comparable with the observed frequency (f_{mhd}) of MHD activity. We note that equilibrium flow velocities in the presence of strong neutral beam injection (NBI) can become strongly sheared and comparable in magnitude with the sound speed. [14] Under these circumstances it is possible for MHD modes to couple to slow magneto-acoustic waves[15]—such behavior is, of course, completely beyond the scope of this paper.

For typical COMPASS-C[3] parameters ($S \sim 10^6$, $\tau_H \sim 10^{-7}$ sec, $f_{mhd} \sim 15$ kHz), we find that

$$Q \sim 100,$$
$$|\gamma_e|/\omega_* \sim 10^{-3}, \qquad (32)$$
$$|\gamma_{i,g}|/\omega_* \sim 10^{-8}.$$

The above figures imply that, in modern-day tokamaks, the amount of reconnected flux induced by an externally applied resonant magnetic perturbation is likely to be reduced by about two orders of magnitude by rotation effects (this corresponds to a reduction in island size by an order of magnitude). Full reconnection (i.e., $\Psi = \Psi_c$) can, however, be achieved close to the electron resonance (i.e., $\Omega' = \omega_{*e}$), but the relative width of this resonance (i.e., $|\gamma_e|/\omega_*$) is fairly small. We note that the ion and low-frequency resonances are so narrow, and the reconnection rates associated with them so small, that they are likely to be completely unobservable.

Of course, the above results only hold in the linear regime, where the island size is much less than the linear layer width. In the next section we consider the extension of these results into the nonlinear regime.

III. NONLINEAR THEORY OF FORCED RECONNECTION IN ROTATING PLASMAS

A. Introduction

In the previous section we showed how the *linear* theory of forced reconnection in a rotating plasma can be constructed as a fairly straightforward extension of the linear theory presented in Ref. 8 for the case of a stationary plasma. Reference 8 also contains a *nonlinear* theory of forced reconnection, in which the island "width" w [defined in Eq. (39)] is found to evolve in time according to the formula

$$I_1 \tau_R \frac{d}{dt}\left(\frac{w}{r_s}\right) = (-\Delta_0' r_s)\left[\left(\frac{w_c}{w}\right)^2 - 1\right] \qquad (33)$$

(in our notation), where $I_1 = 2.326$, τ_R is the local resistive time-scale, and w_c is the island "width" associated with the reconnected flux Ψ_c. In this section, we shall generalize Eq. (33) to the case where the plasma is rotating.

The formula (33) was derived using the standard Rutherford theory[16] for the evolution of a stationary, constant-ψ magnetic island in slab geometry. In order to make any further progress we must now extend this theory to the case where the magnetic island propagates through the plasma with a substantial velocity (i.e., the case where the island has a real frequency $\omega \gg \tau_R^{-1}$). As is made clear in the following paragraph, this extension is by no means straightforward.

Consider the situation in the local $\mathbf{E} \wedge \mathbf{B}$ frame of the unperturbed plasma. The plasma inside the island can only leak across the separatrix on a comparatively slow resistive time scale. So, to a first approximation, it is forced to corotate with the island (at a velocity $\omega/k_\theta - u_{eq}$). The plasma many island widths away from the separatrix is, of course, stationary (assuming that the island is thin, i.e., $w/r_s \ll 1$), but viscous coupling between the plasma inside and outside the separatrix tends to set up a sheared flow pattern in the immediate vicinity of the island. Now, the island and its associated flow pattern propagate through the plasma with a velocity that greatly exceeds the typical velocity with which plasma can flow across magnetic field lines under the influence of resistivity. It follows that, to a first approximation, the island flow must be governed by *ideal* MHD. Given this, plus the fact that the topology of the magnetic field lines changes abruptly at the island separatrix, it is inevitable that the topology of the flow pattern will also change abruptly at the separatrix. Note, however, that such abrupt changes in the flow will be strenuously resisted by viscosity, leading to the formation of a boundary layer on the separatrix. It turns out that the comparatively large gradients which exist in this boundary layer allow advective inertia, which is otherwise negligible, to play an important role in coupling the various flows inside and outside the separatrix. It can be seen, then, that the flow pattern set up around a propagating island is determined by a very complex interaction between the changing topology of the magnetic field, on the one hand,

and the plasma viscosity and inertia, on the other. The ideal flows in the vicinity of the island induce circulatory currents which, depending on their phase, can give rise to a torque modifying the island frequency ω, or a body force modifying the island width w.

There are, of course, plasma flows associated with the expansion of a (stationary) Rutherford island, but since this expansion takes place on a resistive time-scale, these flows are governed by *resistive* MHD and are not, therefore, constrained by the change in topology of the magnetic field at the separatrix. In particular, there is no need for any viscous boundary layer to link the flows inside and outside the separatrix. (Note that there is, in fact, a boundary layer close to the X points, but this has no discernible effect on the island evolution).[17] It follows that the flows around a Rutherford island are not especially complicated (except in the vicinity of the X points) and no circulating currents are induced. In fact, these flows do not even have to be explicitly calculated in order to obtain Rutherford's island evolution equation.

Toward the end of this section, we obtain equations determining the time evolution of the island width, w, and frequency, ω, as part of an extremely complex time-dependent system, which we shall make no attempt to solve in this paper. Fortunately, however, in the case of forced reconnection this system reduces, with the assumption of a steady-state flow pattern, to just a pair of equations determining the width and relative phase of the island. The equation for the island width evolution is similar to Eq. (33), except that it contains a *stabilizing* rotation term which scales approximately like w^{-3}.

B. Basic definitions

In cylindrical geometry the magnetic field is written

$$\mathbf{B} = B_z \hat{\mathbf{z}} + \nabla(\psi_{eq} + \psi_1) \wedge \hat{\mathbf{z}}, \qquad (34)$$

where $\hat{\mathbf{z}}$ is the unit symmetry axis. A low-beta, tokamak ordering is assumed, with $B_z \gg B_\theta$ and negligible poloidal currents. Consequently, B_z can be treated as approximately constant. In Eq. (34), ψ_{eq} is the equilibrium poloidal flux (assumed to be time-independent), and ψ_1 is the perturbed poloidal flux.

The electric field takes the form

$$\mathbf{E} = -\frac{1}{c}\frac{\partial \psi_1}{\partial t}\hat{\mathbf{z}} - \nabla\phi, \qquad (35)$$

where c is the velocity of light and ϕ the electric potential.

The same set of cylindrical coordinates is used as in Sec. II, however in the following it is generally convenient to transform to the right-handed set of flux-surface coordinates χ, θ, and ξ, where

$$\chi = \tfrac{1}{2}(B_z/l_s)x^2 + \psi_1 \qquad (36)$$

is the helical flux and

$$\xi = m\theta - n\zeta - \varphi(t) \qquad (37)$$

is the helical angle. Here, $l_s = (Rq^2/rq')_{r_s}$ is the magnetic shear length at the rational surface and φ is the time-dependent phase of the perturbation. In the following, all quantities are assumed to be functions of χ and ξ only—this is

reasonable in cylindrical geometry. Note that $\mathbf{B}\cdot\nabla\chi \equiv 0$ and $\nabla\xi \equiv \mathbf{k}$, where $\mathbf{k}$ is the wave vector of the perturbation. The rational surface, radius r_s, is defined as the locus of $\mathbf{k}\cdot\mathbf{B} = 0$. In the vicinity of the rational surface, $\mathbf{k}\cdot\mathbf{B}/B \equiv k_\| \sim -(k_\theta/l_s)x$, where $x = r - r_s$.

It is assumed that the magnetic perturbation is dominated by a single harmonic [i.e., the (m, n) harmonic] and lies in the so-called "constant-ψ" regime. Thus, the perturbed flux takes the form

$$\psi_1 = \Psi(t)\cos\xi \qquad (38)$$

with $\Psi > 0$. The single harmonic approximation is particularly appropriate to the problem of forced reconnection, where the Δ' of the driven harmonic becomes positive whilst the Δ's of all the other harmonics remain negative. A necessary condition for the validity of the constant-ψ approximation is that the fractional change in the perturbed poloidal flux across the island, $\delta\psi_1/\psi_1$, should be fairly small. From the definition of Δ', this implies $\delta\psi_1/\psi_1 \sim (w/r_s)(\Delta' r_s) \ll 1$, which is clearly valid for thin islands provided $\Delta' r_s$ is not excessively large. We note that in the initial stages of forced reconnection, which generally lie in the linear regime, $\Delta' r_s$ can become extremely large, but by the time the system enters the nonlinear regime $\Delta' r_s$ has usually dropped to fairly moderative values that are consistent with the constant-ψ approximation. Another requirement for the validity of the constant-ψ approximation is that the resistive skin diffusion rate across the island should be much larger than any oscillation/evolution rate;[16] this implies the rather restrictive condition $(\omega\tau_R) \ll (r_s/w)^2$.

It is convenient to define the island "width" w as follows:

$$w = (2l_s/B_z)^{1/2}\Psi^{1/2}. \qquad (39)$$

In fact, the "true" width (i.e., the maximum width of the region of reconnected flux) is $2\sqrt{2}$ times w. Note again that the island is assumed to be thin—i.e., $w \ll r_s$. It is useful to define a scaled radial flux coordinate

$$\Omega = \chi/\Psi = X^2 + \cos\xi, \qquad (40)$$

where

$$x = \sigma\omega X, \quad \sigma = \text{sgn}(x), \quad X = (\Omega - \cos\xi)^{1/2}. \qquad (41)$$

The island separatrix lies at $\Omega = 1$ and the O point at $\Omega = -1$.

C. The Nonlinear island equations

The following simple set of collisional nonlinear island equations can be derived from the Braginskii[18] two-fluid equations:

$$-\eta_\| j_{\|1} = \frac{1}{c}\frac{\partial\psi_1}{\partial t}\bigg|_{x,\theta,\zeta} + \nabla_\|\phi_1,$$

$$\nabla_\| j_{\|1} = \left(\frac{c^2}{4\pi v_A^2}\right)\left(\frac{\partial}{\partial t}\bigg|_{x,\theta,\zeta} + \mathbf{v}_\perp\cdot\nabla - \nu_\perp\nabla_\perp^2\right)\nabla_\perp^2\phi_1. \qquad (42)$$

Here, $\eta_\|$ is the parallel electrical conductivity, $\nu_\perp$ is the coefficient of perpendicular ion viscosity, and $v_A = (B_z^2/4\pi\rho)^{1/2}$ is the Alfvén velocity. The local $\mathbf{E}\wedge\mathbf{B}$ velocity is written

$$\mathbf{v}_\perp = (c/B_z)\hat{\mathbf{z}}\wedge\nabla\phi_1. \qquad (43)$$

In the above, the electric potential is expanded $\phi \simeq \phi_{eq} + \phi_1$, where $\phi_1 \to (\partial \phi_{eq}/\partial r)x$ for $|x| \gg w$. We assume that $\phi_1/\phi_{eq} \sim w/r_s \ll 1$ in the vicinity of the island. Here, ϕ_{eq} and $(\partial \phi_{eq}/\partial r)$ are constants evaluated at $r = r_s$.

The Ampère–Maxwell equation yields

$$j_{\|1} \simeq -\frac{c}{4\pi}\frac{\partial^2 \psi_1}{\partial x^2} \qquad (44)$$

for thin islands. Here, $j_{\|1}$ is the perturbed parallel current.

The boundary conditions applicable to Eqs. (42) are

$$\phi_1 \to -xE_r \quad \text{as } |x|/w \to \infty, \qquad (45)$$

where $E_r = -(\partial \phi_{eq}/\partial r)$, and

$$\int_{-\pi}^{\pi} \frac{d\xi}{2\pi}\int_{-\infty}^{\infty} dx\left(-\frac{8\pi}{c}j_{\|1}\right)\cos\xi = \mathrm{Re}(\Delta')\Psi, \quad (46a)$$

$$\int_{-\pi}^{\pi} \frac{d\xi}{2\pi}\int_{-\infty}^{\infty} dx\left(-\frac{8\pi}{c}j_{\|1}\right)\sin\xi = -\mathrm{Im}(\Delta')\Psi, \quad (46b)$$

Equations (46) follow from the usual definition of Δ'—i.e., that it is the jump in the logarithmic derivative of ψ_1 across the layer.[10]

Equations (42) can be obtained from Eqs. (1)–(4) of Scott and Hassam[19] by neglecting all semicollisional and diamagnetic terms, and adding in a term describing the action of perpendicular ion viscosity. The more general equations of Biskamp[20] also reduce to Eqs. (42) under similar circumstances, provided that the island is thin.

It is straightforward to show (e.g., by an examination of the relative orders of magnitude of the various terms in the equations of Scott and Hassam) that the neglect of semicollisional terms in Eqs. (42) is justified once the island width w greatly exceeds the scale length $\rho_s = (T_e m_i/Z)^{1/2}(c/eB_z)$. Electron diamagnetic effects become unimportant when the island size exceeds the scale length $\rho_s(l_s/l_n)$ (where l_n is the local density scale length), because beyond this critical island size ion sound waves can effectively iron out any pressure fluctuations around flux surfaces.[21] There is, however, no justification in general for the neglect of ion diamagnetic effects in Eqs. (42), because of the strong viscous coupling expected between the ion fluid and the perturbed magnetic field. It follows, therefore, that our nonlinear island equations are only valid when ion diamagnetic effects are unimportant (e.g., if $T_i \ll T_e$). By analogy with the linear regime, where ion diamagnetic rotation was found to be similar in effect to $\mathbf{E} \wedge \mathbf{B}$ rotation (apart from a reduction in the rate of reconnection), we do not expect this restriction to qualitatively affect our nonlinear results. Note, finally, that all finite-Larmor-radius effects have been neglected in Eqs. (42). This is obviously reasonable provided that $w \gg \rho_i$, where ρ_i is the ion Larmor radius.

The above considerations lead us to the conclusion that Eqs. (42) are valid in slab geometry provided that the constant-ψ approximation holds and the following two inequalities are satisfied:

$$\rho_i, \ \rho_s, \ \rho_s(l_s/l_n) \ll w \ll r_s,$$
$$T_i \ll T_e. \qquad (47)$$

D. Operators and derivatives

Let

$$\nabla_\| \equiv \mathbf{b}\cdot\nabla = \mathbf{b}\cdot\mathbf{k}\frac{\partial}{\partial\xi} = -\sigma w\frac{k_\theta}{l_s}X\frac{\partial}{\partial\xi},$$

$$\nabla_\perp^2 f \equiv \nabla\cdot(\nabla f - \nabla_\| f \mathbf{b}) \simeq \frac{4}{w^2}\left(X^2\frac{\partial^2}{\partial\Omega^2} + \frac{1}{2}\frac{\partial}{\partial\Omega}\right)f, \qquad (48)$$

where $\mathbf{b}\equiv\mathbf{B}/|B|$ and f is an arbitrary function. Now

$$\frac{\partial}{\partial t}\Big|_{x,\theta,\zeta} \equiv \frac{\partial}{\partial t} + \frac{\partial\Omega}{\partial t}\Big|_{x,\theta,\zeta}\frac{\partial}{\partial\Omega} + \frac{\partial\xi}{\partial t}\Big|_{x,\theta,\zeta}\frac{\partial}{\partial\xi}, \qquad (49)$$

so

$$\frac{\partial}{\partial t}\Big|_{x,\theta,\zeta} \equiv \frac{\partial}{\partial t} + (-2\gamma X^2 + \omega\sin\xi)\frac{\partial}{\partial\Omega} - w\frac{\partial}{\partial\xi}, \qquad (50)$$

where

$$\gamma = \frac{d}{dt}(\ln w),$$
$$\omega = \frac{d\varphi}{dt}. \qquad (51)$$

Also,

$$\mathbf{v}_\perp\cdot\nabla \equiv \sigma\frac{2}{w}\frac{ck_\theta}{B_z}X\left(\frac{\partial\phi_1}{\partial\Omega}\frac{\partial}{\partial\xi} - \frac{\partial\phi_1}{\partial\xi}\frac{\partial}{\partial\Omega}\right). \qquad (52)$$

Any general function $f(\sigma,\Omega,\xi)$ can be written as a sum of even and odd (in x) terms as follows:

$$f(\sigma,\Omega,\xi) = f_+(\Omega,\xi) + \sigma f_-(\Omega,\xi). \qquad (53)$$

The flux-surface average operator is defined

$$\langle f(\sigma,\Omega,\xi)\rangle \equiv \frac{1}{2\pi}\int_{\xi_0}^{2\pi-\xi_0}\frac{f_+(\Omega,\xi)}{X}d\xi, \quad \Omega < 1,$$

$$\langle f(\sigma,\Omega,\xi)\rangle \equiv \frac{1}{2\pi}\oint\frac{f(\Omega,\xi)}{X}d\xi, \quad \Omega > 1, \qquad (54)$$

where $\xi_0(\Omega)$ satisfies both $0\leqslant\xi_0\leqslant\pi$ and $X(\Omega,\xi_0) = 0$. It follows from (54) that

$$\langle f\rangle = \langle f_+\rangle, \quad \text{for } \Omega < 1,$$
$$\langle \sigma f\rangle = \langle f_-\rangle, \quad \text{for } \Omega < 1. \qquad (55)$$

Note that

$$\left\langle \sigma X\frac{\partial f}{\partial\xi}\right\rangle = \left\langle X\frac{\partial f}{\partial\xi}\right\rangle = 0, \quad \text{for } \Omega > 1, \qquad (56)$$

but

$$\left\langle \sigma X\frac{\partial f}{\partial\xi}\right\rangle = \frac{1}{2\pi}[f_-(2\pi-\xi_0) - f_-(\xi_0)], \quad \text{for } \Omega < 1,$$

$$\left\langle X\frac{\partial f}{\partial\xi}\right\rangle = \frac{1}{2\pi}[f_+(2\pi-\xi_0) - f_+(\xi_0)], \quad \text{for } \Omega < 1. \qquad (57)$$

Any general function $f(\Omega,\xi)$ can be written as a sum of flux-surface average and oscillating terms as follows:

$$f(\Omega,\xi) = \bar{f}(\Omega) + \tilde{f}(\Omega,\xi), \qquad (58)$$

where $\bar{f}(\Omega) \equiv \langle f\rangle/\langle 1\rangle$ and $\langle\tilde{f}\rangle \equiv 0$.

The function $\Theta(\Omega,\xi)$ is defined (inside the separatrix) as

$$\Theta(\Omega,\xi) = -\frac{1}{\sqrt{2}}\int_\pi^\xi \frac{d\xi'}{X}. \tag{59}$$

It follows from (59) that

$$\Theta\frac{\partial f}{\partial \xi} \equiv \frac{\partial}{\partial \xi}(\Theta f) + \frac{1}{\sqrt{2}}\frac{f}{X}. \tag{60}$$

Equations (54), (57), (59), and (60) imply that inside the separatrix

$$\left\langle \Theta X\frac{\partial f}{\partial \xi}\right\rangle \equiv \frac{1}{\sqrt{2}}\left(\langle f_+ \rangle - \frac{1}{2}\right.$$
$$\left. \times [f_+(2\pi-\xi_0)+f_+(\xi_0)]\langle 1\rangle\right),$$

$$\left\langle \sigma\Theta X\frac{\partial f}{\partial \xi}\right\rangle \equiv \frac{1}{\sqrt{2}}\left(\langle f_- \rangle - \frac{1}{2}\right.$$
$$\left. \times [f_-(2\pi-\xi_0)+f_-(\xi_0)]\langle 1\rangle\right). \tag{61}$$

Similarly, it can be shown that

$$\left\langle X^2\frac{\partial f}{\partial \xi}\right\rangle = -\frac{1}{2}\langle f_+ \sin\xi\rangle,$$

$$\left\langle \sigma X^2\frac{\partial f}{\partial \xi}\right\rangle = -\frac{1}{2}\langle f_- \sin\xi\rangle, \tag{62}$$

and

$$\left\langle \Xi X\frac{\partial f}{\partial \xi}\right\rangle = \frac{1}{\sqrt{2}}\langle \tilde{f}_+ \cos\xi\rangle,$$

$$\left\langle \sigma\Xi X\frac{\partial f}{\partial \xi}\right\rangle = \frac{1}{\sqrt{2}}\langle \tilde{f}_- \cos\xi\rangle, \tag{63}$$

where

$$\Xi(\Omega,\xi) = -\frac{1}{\sqrt{2}}\int_\pi^\xi \frac{\widetilde{\cos\xi'}}{X}\,d\xi'. \tag{64}$$

E. The normalized island equations

Making use of some of the above definitions, Eqs. (42) can be normalized to give

$$\frac{1}{\tau_R}\left(\frac{r_s}{w}\right)J = \left(\gamma\cos\xi + \frac{1}{2}\omega\sin\xi\right) - \sigma X\frac{\partial\hat{\phi}}{\partial\xi},$$

$$\sigma X\frac{\partial J}{\partial\xi} = 8\tau_H^2\left(\frac{r_s}{w}\right)^3\left[\frac{1}{2}\frac{\partial}{\partial t} - \frac{1}{2}\gamma + \left(-\gamma X^2\right.\right.$$
$$\left. + \frac{1}{2}\omega\sin\xi\right)\frac{\partial}{\partial\Omega} - \frac{1}{2}\omega\frac{\partial}{\partial\xi} + \sigma X\left(\frac{\partial\hat{\phi}}{\partial\Omega}\frac{\partial}{\partial\xi}\right.$$
$$\left.\left. - \frac{\partial\hat{\phi}}{\partial\xi}\frac{\partial}{\partial\Omega}\right)\right] - \left(\frac{2\nu_\perp}{w^2}\right)\hat{\nabla}_\perp^2\right]\hat{\nabla}_\perp^2\hat{\phi}, \tag{65}$$

where

$$\phi_1 = (B_z/ck_\theta)w\hat{\phi},$$
$$j_{\|1} = -(cB_z/4\pi l_s r_s)wJ,$$
$$\hat{\nabla}_\perp^2 = \left(X^2\frac{\partial^2}{\partial\Omega^2} + \frac{1}{2}\frac{\partial}{\partial\Omega}\right),$$
$$\tau_H = l_s/m v_A,$$
$$\tau_R = r_s^2\left(\frac{\eta_\| c^2}{4\pi}\right)^{-1}. \tag{66}$$

The normalized island boundary conditions can be written

$$\hat{\phi}_- \to (k_\theta u_{eq})X \quad \text{as } X\to\infty,$$
$$\hat{\phi}_+ \to 0 \quad \text{as } X\to\infty, \tag{67}$$

and

$$\int_{-1}^\infty d\Omega\langle J_+ \cos\xi\rangle = \frac{1}{4}\text{Re}(\Delta'r_s),$$

$$\int_{-1}^\infty d\Omega\langle J_+ \sin\xi\rangle = -\frac{1}{4}\text{Im}(\Delta'r_s), \tag{68}$$

where

$$u_{eq} = -cE_r/B_z \tag{69}$$

is the $\mathbf{E}\wedge\mathbf{B}$ velocity of the unperturbed plasma at the rational surface.

Let

$$\hat{\phi}(\sigma,\Omega,\xi) = \sigma[\omega X + \gamma g(\Omega,\xi)] + \omega_\nu\mathcal{H}(\sigma,\Omega,\xi), \tag{70}$$

where

$$\omega_\nu = 2\nu_\perp/w^2 \tag{71}$$

is the viscous diffusion rate across the island. The function $\mathcal{H}$ is (almost) the normalized electric potential in the frame of reference in which the island is stationary. The function g represents the resistive flows induced by island growth or shrinkage, and takes the form

$$g(\Omega,\xi) = \int_\pi^\xi \frac{\widetilde{\cos\xi'}}{X}\,d\xi'. \tag{72}$$

The boundary conditions (67) imply that

$$\mathcal{H}_- \to \left(\frac{k_\theta u_{eq}-\omega}{\omega_\nu}\right)\Omega^{1/2} \quad \text{as } \Omega\to\infty, \tag{73}$$

with

$$\mathcal{H}_+ \to 0 \quad \text{as } \Omega\to\infty. \tag{74}$$

Equations (65) can be written

$$\frac{1}{\tau_R}\left(\frac{r_s}{w}\right)\bar{J}_+ = \gamma\frac{\langle\cos\xi\rangle}{\langle 1\rangle}, \tag{75a}$$

$$\frac{1}{(\tau_R\omega_\nu)}\left(\frac{r_s}{w}\right)(\bar{J}_+ + \sigma J_-) = -\sigma X\frac{\partial\mathcal{H}}{\partial\xi}, \tag{75b}$$

$$\sigma X\frac{\partial}{\partial\xi}(\bar{J}_+ + \sigma J_-)$$
$$= 8\tau_H^2\left(\frac{r_s}{w}\right)^3\left[\frac{1}{2}\frac{\partial}{\partial t} + \gamma\left(-\frac{1}{2} - \frac{\langle X^2\rangle}{\langle 1\rangle}\frac{\partial}{\partial\Omega}\right.\right.$$
$$\left. + X\frac{\partial g}{\partial\Omega}\frac{\partial}{\partial\xi}\right) + \omega_\nu\sigma X\left(\frac{\partial\mathcal{H}}{\partial\Omega}\frac{\partial}{\partial\xi} - \frac{\partial\mathcal{H}}{\partial\xi}\frac{\partial}{\partial\Omega}\right)$$
$$\left. - \omega_\nu\hat{\nabla}_\perp^2\right]\hat{\nabla}_\perp^2\hat{\phi}. \tag{75c}$$

Equations (75b) and (75c) can be combined to give

$$X\frac{\partial}{\partial\xi}X\frac{\partial}{\partial\xi}\mathcal{H}$$

$$= -\frac{8}{(\omega_v\omega_*)}\left(\frac{\Delta_c}{w}\right)^4$$

$$\times\left[\frac{1}{2}\frac{\partial}{\partial t}+\gamma\left(-\frac{1}{2}-\frac{\langle X^2\rangle}{\langle 1\rangle}\frac{\partial}{\partial\Omega}+X\frac{\partial g}{\partial\Omega}\frac{\partial}{\partial\xi}\right)\right.$$

$$\left.+\omega_v\sigma X\left(\frac{\partial\mathcal{H}}{\partial\Omega}\frac{\partial}{\partial\xi}-\frac{\partial\mathcal{H}}{\partial\xi}\frac{\partial}{\partial\Omega}\right)-\omega_v\hat{\nabla}_\perp^2\right]\hat{\nabla}_\perp^2\hat{\phi}, \quad (76)$$

where $\Delta_c = (\omega_*\tau_H^2/\tau_R)^{1/4}r_s$ is the typical linear layer width of a collisional drift-tearing mode of typical real frequency ω_*. (N.B. ω_* is generally of order the electron diamagnetic frequency.)

It follows from Eqs. (73), (74), and (76) that

$$\mathcal{H} = \mathcal{H}_{(0)} + \tilde{\mathcal{H}}_{(1)}, \quad (77)$$

where

$$\mathcal{H}_{(0)} \sim O(\omega_*/\omega_v) \quad (78)$$

and

$$\tilde{\mathcal{H}}_{(1)} \sim \left(\frac{\Delta_c}{w}\right)^4\left(\frac{\omega_*}{\omega_v}\right)$$

$$\times\left[O\left(\frac{dw/dt}{\omega_*^2}\right), O\left(\frac{\gamma}{\omega_*}\right), O(\tilde{H}_{(1)}), O\left(\frac{\omega_v}{\omega_*}\right)\right]. \quad (79)$$

[Here, it has been assumed that $\omega \sim (k_\theta u_{\text{eq}}) \sim \omega_*$.] Suppose the various frequencies and length scales in the system are ordered such that

$$\left(\frac{\gamma}{\omega_*}\right), \quad \tilde{\mathcal{H}}_{(1)} \ll \left(\frac{dw/dt}{\omega_*^2}\right), \quad \left(\frac{\omega_v}{\omega_*}\right), \quad (80)$$

then Eqs. (70), (75), and (76) yield the following form for the vorticity evolution equation:

$$X\frac{\partial}{\partial\xi}X\frac{\partial}{\partial\xi}\mathcal{H}$$

$$= -\frac{1}{(\omega_v\tau_R)}\left(\frac{r_s}{w}\right)\sigma X\frac{\partial}{\partial\xi}(\tilde{J}_+ + \sigma J_-)$$

$$= -\frac{\lambda^4}{8}\left[\frac{\partial}{\partial T}+\sigma X\left(\frac{\partial\mathcal{H}_{(0)}}{\partial\Omega}\frac{\partial}{\partial\xi}\right.\right.$$

$$\left.\left.-\frac{\partial\mathcal{H}_{(0)}}{\partial\xi}\frac{\partial}{\partial\Omega}\right)-\hat{\nabla}_\perp^2\right]\hat{\nabla}_\perp^2\mathcal{H}_{(0)}, \quad (81)$$

where

$$\gamma = \sqrt{8}\left(\frac{\omega_v}{\omega_*}\right)^{1/4}\left(\frac{\Delta_c}{w}\right) = \sqrt{8}\left(\frac{\omega_s\tau_H^2}{\tau_R}\right)^{1/4}\left(\frac{r_s}{w}\right)^{3/2},$$

$$\omega_s = 2\nu_\perp/r_s^2,$$

$$T = (2\omega_v)t. \quad (82)$$

Here, ω_s is the viscous diffusion rate across length scales comparable with the minor radius and T is the time normalized with respect to the viscous diffusion rate across the island. The first term in the square brackets on the right-hand side of (81) corresponds to ion polarization drift, the second to advective inertia, and the third to perpendicular ion viscosity. It follows from (47), (80), and the assumption of constant ψ, that Eq. (81) is valid provided:

(1) The island width is much greater than any microscopic scale length or typical linear layer width, but much less than any macroscopic scale length (e.g., the minor radius):

$$\rho_i, \rho_s, \rho_s(l_s/l_n), \Delta_c \ll w \ll r_s. \quad (83)$$

(2) The ions are cold:

$$T_i \ll T_e. \quad (84)$$

(3) The fractional change in the perturbed poloidal flux across the island is small (this is necessary for the validity of the constant-ψ approximation):

$$(w/r_s) \ll 1/(\Delta'r_s). \quad (85)$$

(4) The magnetic Reynolds number, $S = \tau_R/\tau_H$, of the plasma is large enough that resistive flows can be neglected with respect to $E\wedge B$ flows and viscous flows, but small enough to be fully consistent with the constant-ψ approximation:

$$\frac{1}{(\omega\tau_H)}, \quad \frac{1}{(\omega_*\tau_H)}, \quad \frac{1}{(\omega_v\tau_H)} \ll S \ll \frac{1}{(\omega\tau_H)}\left(\frac{r_s}{w}\right)^2. \quad (86)$$

In the following, it is assumed that $\lambda \ll 1$, so that from (81) inertia and viscosity are negligible to lowest order except in those regions where the local gradients become extremely large (i.e., in boundary layers).

F. The outer solution

The "outer" region, which comprises most of the plasma, is defined as that region in which inertia and viscosity can be neglected to lowest order. The "inner" region consists of a number of thin viscous boundary layers that are necessary in order to link up the flow in the various outer regions continuously.

On the assumption that all derivatives in Ω and ξ are $O(1)$, the potential $\mathcal{H}$ can be expanded as follows:

$$\mathcal{H}(\sigma,\Omega,\xi) = \sum_{n=0}^{\infty}\lambda^{4n}\mathcal{H}_{(n)}(\sigma,\Omega,\xi). \quad (87)$$

Equation (81) implies that

$$X\frac{\partial}{\partial\xi}X\frac{\partial}{\partial\xi}\mathcal{H}_{(0)} = 0, \quad (88)$$

yielding

$$\mathcal{H}_{(0)}(\sigma,\Omega,\xi) = \bar{h}_+(\Omega)$$

$$+\sigma\bar{h}_-(\Omega), \quad \Omega > 1,$$

$$\mathcal{H}_{(0)}(\sigma,\Omega,\xi) = \bar{h}_+(\Omega) + \bar{f}(\Omega)$$

$$+\bar{F}(\Omega)\Theta(\Omega,\xi), \quad \Omega < 1, \quad (89)$$

where $\bar{h}_+$ and all its derivatives are continuous at the separatrix. Note that $\bar{h}_-$ must be zero inside the separatrix by symmetry. The function $\bar{F}$ must be zero outside the separatrix because $\Theta(\Omega,\xi)$ is not a periodic function of ξ for $\Omega > 1$.

The boundary conditions

$$\bar{h}_-(1) = \bar{f}(1) = \bar{F}(1) = 0 \quad (90)$$

ensure that $\mathcal{H}_{(0)}$ is continuous at the separatrix. Note, however, that in general the derivatives of $\mathcal{H}_{(0)}$ are discontinuous at $\Omega = 1$. Such discontinuities are resolved by the pres-

ence of a viscous boundary layer, of thickness (in Ω) λ, at the separatrix.

Equations (89) imply that the zero-order flow in the outer region is described by three flux functions, $\bar{h}_-(\Omega)$, $\bar{f}(\Omega)$, and $\overline{F}(\Omega)$, which correspond to three distinct types of motion. [N.B. There is, in fact, a fourth flux function, $\bar{h}_+(\Omega)$, but this turns out to be much less important than the other three, so for the time being it will be neglected.] The flow patterns associated with the various flux functions are sketched in Fig. 6. It can be seen that $\bar{h}_-$ corresponds to even (in x) flow around flux surfaces outside the separatrix, while $\bar{f}$ corresponds to circulation around flux surfaces inside the separatrix, and finally, $\overline{F}$ corresponds to a convection-cell type flow pattern inside the separatrix. Note that there are discontinuous jumps in $\mathbf{v}_\perp \cdot \mathbf{k}$ at $X = 0$ in the convection-cell pattern—this occurs because $(\partial\Theta/\partial X)_\xi \neq 0$ at $X = 0$. Such unphysical behavior is averted by the presence of a thin viscous boundary layer at $X = 0$.

From Eqs. (73) and (74), the boundary conditions satisfied by $\mathcal{H}_{(0)}$ are

$$\bar{h}_- \to [(k_\theta u_{eq} - \omega)/\omega_v]\Omega^{1/2} \quad \text{as } \Omega \to \infty,$$
$$\bar{h}_+ \to 0 \quad \text{as } \Omega \to \infty. \tag{91}$$

It follows that since the potential $\bar{h}_+$ is not driven by the external boundary conditions it will rapidly decay away under the action of perpendicular ion viscosity. It would, therefore, seem reasonable to take

$$\bar{h}_+ = 0 \tag{92}$$

for all Ω. As will become apparent later on, $\bar{f}$ and $\overline{F}$ are driven, via the viscous boundary layer at the separatrix, by the external boundary condition on $\bar{h}_-$.
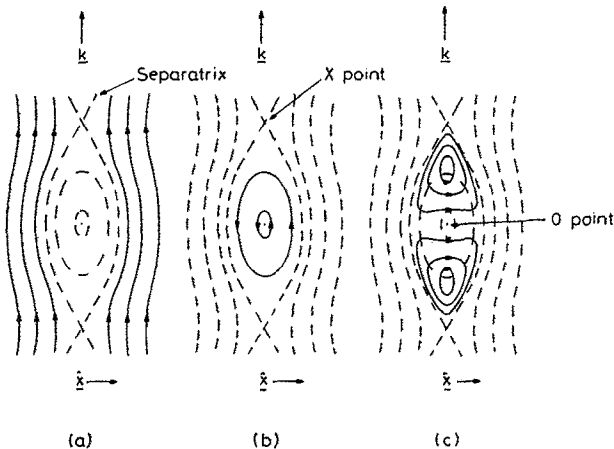

FIG. 6. A sketch of the three possible types of zero-order flow in the vicinity of the magnetic island. A cross section of the $\mathbf{k}$-$\hat{x}$ plane is shown in the neighborhood of the rational surface. Here, $\mathbf{k}$ is the wave vector of the perturbation and $\hat{x}$ is the unit vector in the x (i.e., radial) direction. The dashed lines represent magnetic flux surfaces, while the solid lines represent flow stream lines. The whereabouts of the island separatrix, and the X and O points are indicated. The first type of motion (a), associated with the potential $\bar{h}_-(\Omega)$, consists of even (in x) flow around flux surfaces outside the separatrix. The second type of motion (b), associated with the potential $\bar{f}(\Omega)$, consists of circulatory flow around flux-surfaces inside the separatrix. The final type of motion (c), associated with the potential $\overline{F}(\Omega)$, consists of convection-cell-type flow inside the separatrix.

G. The time evolution of the outer solution

1. Flow outside the separatrix

From (56), (89), and symmetry, the flux-surface average of Eq. (81) yields

$$\frac{\partial}{\partial T}\overline{\nabla}_\perp^2 \bar{h}_- - \overline{\nabla}_\perp^4 \bar{h}_- = 0 \tag{93}$$

for $\Omega \geqslant 1$, where

$$\overline{\nabla}_\perp^2 \equiv \frac{\langle \hat{\nabla}_\perp^2 \rangle}{\langle 1 \rangle} = A_0(\Omega)\frac{\partial^2}{\partial\Omega^2} + \frac{1}{2}\frac{\partial}{\partial\Omega},$$

$$\overline{\nabla}_\perp^4 \equiv \frac{\langle \hat{\nabla}_\perp^4 \rangle}{\langle 1 \rangle} = A_1(\Omega)\frac{\partial^4}{\partial\Omega^4} + 3A_0(\Omega)\frac{\partial^3}{\partial\Omega^3} + \frac{3}{4}\frac{\partial^2}{\partial\Omega^2}, \tag{94}$$

with $\hat{\nabla}_\perp^4 \equiv \hat{\nabla}_\perp^2 \hat{\nabla}_\perp^2$. Here, $A_0(\Omega)$ and $A_1(\Omega)$ are flux-surface average quantities specified in the Appendix. Equations (91) and (93) describe how the vorticity associated with even flow outside the separatrix tends to decay away under the action of perpendicular ion viscosity, but is sustained by the external boundary conditions.

2. Flow inside the separatrix

Inside the separatrix the even portion of Eq. (81) takes the form

$$\left(\frac{8}{\lambda^4}\right)\frac{1}{(\omega_v\tau_R)}\left(\frac{r_s}{w}\right)X\frac{\partial J_-}{\partial\xi}$$
$$= \left(\frac{\partial}{\partial T}\hat{\nabla}_\perp^2\bar{f} - \hat{\nabla}_\perp^4\bar{f}\right) + \left(\frac{\partial}{\partial T}\hat{\nabla}_\perp^2(\Theta\overline{F}) - \hat{\nabla}_\perp^4(\Theta\overline{F})\right), \tag{95}$$

where use has been made of (89). If the following two consistency relations are satisfied:

$$\frac{\partial}{\partial T}\overline{\nabla}_\perp^2\bar{f} - \overline{\nabla}_\perp^4\bar{f} = 0, \tag{96a}$$

$$\frac{\partial}{\partial T}\breve{\nabla}_\perp^2\overline{F} - \breve{\nabla}_\perp^4\overline{F} = 0, \tag{96b}$$

for $\Omega \leqslant 1$, then it is easily shown that J_- takes the form

$$J_-(\Omega,\xi) = \overline{J}_{(0)-}(\Omega) + \tilde{J}_{(1)-}(\Omega,\xi) \tag{97}$$

inside the separatrix, where

$$\tilde{J}_{(1)-} \to 0 \quad \text{as } X \to 0. \tag{98}$$

In the above

$$\breve{\nabla}_\perp^2 \equiv \frac{\langle \Theta\hat{\nabla}_\perp^2\Theta \rangle}{\langle 1 \rangle} = B_2(\Omega)\frac{\partial^2}{\partial\Omega^2} + B_1(\Omega)\frac{\partial}{\partial\Omega} + B_0(\Omega),$$

$$\breve{\nabla}_\perp^4 \equiv \frac{\langle \Theta\hat{\nabla}_\perp^4\Theta \rangle}{\langle 1 \rangle} = C_4(\Omega)\frac{\partial^4}{\partial\Omega^4} + C_3(\Omega)\frac{\partial^3}{\partial\Omega^3}$$
$$+ C_2(\Omega)\frac{\partial^2}{\partial\Omega^2} + C_1(\Omega)\frac{\partial}{\partial\Omega} + C_0(\Omega), \tag{99}$$

where the $B_i(\Omega)$ and the $C_i(\Omega)$ are flux-surface average quantities specified in the Appendix. Note from (75b) and (89) that the zeroth-order odd current distribution $J_{(0)-}(\sigma,\Omega,\xi) \equiv \sigma\overline{J}_{(0)-}(\Omega)$ has the form

$$J_{(0)-}(\sigma,\Omega,\xi) = \sigma(1/\sqrt{2})(\omega_v\tau_R)(w/r_s)\overline{F}(\Omega). \tag{100}$$

The above current distribution is clearly discontinuous at

$X = 0$. Unphysical behavior is averted by the presence of a thin viscous layer, centered on $X = 0$, which ensures that $J_{(0)-}(\sigma,\Omega,\xi)$ is a smoothly varying function at small X. Note that even in the absence of a viscous layer the consistency relations (96) ensure that the first-order odd current distribution $J_{(1)-}(\sigma,\Omega,\xi) \equiv \sigma \tilde{J}_{(1)-}(\Omega,\xi)$ is well-behaved at small X.

Equations (96) describe how the vorticities associated with circulatory flow and convection-cell-type flow inside the separatrix tend to decay away under the action of perpendicular ion viscosity. Both types of flow are ultimately maintained by the external boundary conditions, via the viscous boundary layer at $\Omega = 1$.

H. The inner solution

The inner region consists of two boundary layers, the first at $X = 0$, and the second at $\Omega = 1$, which are needed in order to link the flow patterns in the various outer regions continuously.

1. The behavior at small X

Consider the behavior of the outer solution (89) at small X. It can easily be shown that

$$\mathcal{H}_{(0)}(\sigma,\Omega,\xi) = \bar{f}(\Omega) + \bar{F}(\Omega)\Theta(\Omega,\xi)$$

$$\rightarrow \bar{f}(\Omega) + \bar{F}(\Omega)\left(\frac{\pi}{2} - \frac{\sqrt{2}X}{(1-\Omega)^{1/2}}\right.$$

$$\left. + O(X^2)\right) \qquad (101)$$

as $X \rightarrow 0$ (for $\xi < \pi$). Since $\mathcal{H}_{(0)}$ is an even function of σ inside the separatrix, it follows from Eq. (101) that $(\partial\mathcal{H}_{(0)}/\partial x)_\xi \propto \sigma(\partial\mathcal{H}_{(0)}/\partial X)_\xi$ is discontinuous at $X = 0$. This discontinuity implies a sudden jump in $\mathbf{v}_\perp \cdot \mathbf{k}$ at $X = 0$. Such behavior is clearly unphysical, and is averted by the presence of a viscous boundary layer close to $X = 0$, which acts so as to link the flow in the regions $\sigma > 0$ and $\sigma < 0$ together smoothly.

At small X, the vorticity evolution equation (81) can be written

$$(1-\Omega^2)\frac{\partial^2\mathcal{H}}{\partial y^2}$$

$$= \frac{1}{8}\left[\sigma\lambda\frac{(1-\Omega^2)^{1/2}}{2}\left(\frac{\partial\mathcal{H}}{\partial y}\frac{\partial}{\partial\Omega}\right.\right.$$

$$\left.\left. - \frac{\partial\mathcal{H}}{\partial\Omega}\frac{\partial}{\partial y}\right) + \frac{1}{4}\frac{\partial^2}{\partial y^2}\right]\frac{\partial^2\mathcal{H}}{\partial y^2} + O(\lambda^4), \qquad (102)$$

where $X = \lambda^2 y$. The lowest-order solution of (102) that links up smoothly with the outer solution $\mathcal{H}_{(0)}$ has the form

$$\mathcal{H}_{(0)'}(\sigma,y,\Omega)$$

$$= \bar{f}(\Omega) + \frac{\pi}{2}\bar{F}(\Omega)$$

$$- \bar{F}(\Omega)\frac{\sqrt{2}\lambda^2}{(1-\Omega^2)^{1/2}}\left[y + \frac{(1/32)^{1/2}}{(1-\Omega^2)^{1/2}}\right.$$

$$\left. \times \exp\left(-\frac{(1-\Omega^2)^{1/2}}{(1/32)^{1/2}}y\right)\right] + O(\lambda^4). \qquad (103)$$

Note that the discontinuity in $(\partial\mathcal{H}/\partial x)_\xi$ at $X = 0$ has now been eliminated, but there still remains a discontinuity in $(\partial^3\mathcal{H}/\partial x^3)_\xi$. This discontinuity, and other discontinuities in the higher derivatives, can be eliminated by expanding to higher order in λ. Note, however, that even the lowest-order layer solution (103) is sufficient to eliminate the discontinuity in $J_{(0)-}$ discussed in Sec. III G 2.

It is clear from the above calculations that discontinuous flow at small X can be prevented by a thin viscous boundary layer, whose thickness (in Ω) is $O(\lambda^2)$ well away from the X or O points. As an X or O point is approached, the thickness of the layer increases until eventually, at $\Omega - 1 \sim \lambda^2$ or $\Omega + 1 \sim \lambda^2$ [where the thickness is $O(\lambda)$], the layer ceases to be a boundary layer at all, at which point the solution (103) breaks down. Note that

$$\left(\frac{\partial\mathcal{H}_{(0)'}}{\partial\Omega}\right)_{y=0} \propto \frac{\partial}{\partial\Omega}\left(\frac{\bar{F}(\Omega)}{(1-\Omega^2)}\right) \qquad (104)$$

as the X or O point is approached. It follows that

$\bar{F}(\Omega) \rightarrow 0$ at least as fast as $(\Omega - 1)$ as $\Omega \rightarrow 1$,

$\bar{F}(\Omega) \rightarrow 0$ at least as fast as $(\Omega + 1)$ as $\Omega \rightarrow -1$,   (105)

in order to prevent $\mathbf{v} \cdot \nabla X$ from becoming unphysically large at the X or O points.

2. Behavior close to the separatrix

Consider the behavior of the potential $\mathcal{H}$ close to $\Omega = 1$. Let

$$\Omega - 1 = \lambda p, \qquad (106)$$

and

$$\mathcal{H}_{(0)'}(\sigma, 1 + \lambda p, \xi) = \sigma U(p,\xi) + V(p,\xi) + W(p,\xi), \qquad (107)$$

where

$U(p,\xi) \rightarrow O(\lambda^4)$ as $p \rightarrow -\infty$,

$U(p,\xi) \rightarrow \bar{h}_-(1 + \lambda p) + O(\lambda^4)$ as $p \rightarrow +\infty$,

$V(p,\xi) \rightarrow \bar{f}(1 + \lambda p) + O(\lambda^4)$ as $p \rightarrow -\infty$,

$V(p,\xi) \rightarrow O(\lambda^4)$ as $p \rightarrow +\infty$,

$W(p,\xi) \rightarrow \bar{F}(1 + \lambda p)\Theta(1 + \lambda p,\xi) + O(\lambda^4)$ as $p \rightarrow -\infty$,

$W(p,\xi) \rightarrow O(\lambda^4)$ as $p \rightarrow +\infty$.   (108)

The above boundary conditions ensure that the inner solution $\mathcal{H}_{(0)'}$ links up smoothly with the outer solution $\mathcal{H}_{(0)}$. Note that U and V have the symmetry of $\cos\xi$, whereas W has the symmetry of $\sin\xi$. The functions U, V, and W can be expanded as follows:

$$[U(p,\xi), V(p,\xi), W(p,\xi)]$$

$$= \sum_{n=0}^{\infty}\lambda^n[U_{(n)}(p,\xi), V_{(n)}(p,\xi), W_{(n)}(p,\xi)]. \qquad (109)$$

Equations (90) and (108) imply that

$$U_{(0)} = V_{(0)} = W_{(0)} = 0. \qquad (110)$$

It follows from (81), (107), (108), and (109) that

$$\left(\frac{\partial}{\partial\mu}(1-\mu^2)\frac{\partial}{\partial\mu} - (1-\mu^2)\frac{\partial^4}{\partial p^4}\right)[U_{(1)}, V_{(1)}, W_{(1)}] = 0, \qquad (111)$$

where

$$\mu = \cos(\xi/2).\tag{112}$$

Partial differential equations can also be derived for the higher-order potentials ($U_{(2)}$, $V_{(2)}$, etc.), but these are generally far more complicated than Eq. (111).

The boundary conditions applicable to Eq. (111) are

$$
\begin{aligned}
U_{(1)} &\to 0 \quad \text{as } p \to -\infty, \\
U_{(1)} &\to p\bar{h}\,'_{-}(1) \quad \text{as } p \to +\infty, \\
V_{(1)} &\to p\bar{f}'(1) \quad \text{as } p \to -\infty, \\
V_{(1)} &\to 0 \quad \text{as } p \to +\infty, \\
W_{(1)} &\to p\overline{F}'(1)Q_0(\mu) \quad \text{as } p \to -\infty, \\
W_{(1)} &\to 0 \quad \text{as } p \to +\infty,
\end{aligned}\tag{113}
$$

where $'$ denotes $\partial/\partial\Omega$ and $Q_0(\mu)$ is a standard Legendre function. Note that close to the X points [i.e., $\xi \leqslant O(\lambda^{1/2})$ or $\xi - 2\pi \leqslant O(\lambda^{1/2})$] the expansion underlying Eqs. (111) and (113) breaks down.

It turns out that, to lowest order in $[\ln(\lambda)]^{-1}$, only a knowledge of the *asymptotic behavior* of the inner potentials ($U_{(n)}$, etc.) is required for the determination of the boundary conditions satisfied by the outer potentials ($\bar{h}_{-}$, etc.) at the separatrix. The specification of the boundary conditions to any higher accuracy would require a knowledge of the potentials $U_{(1)}$, $V_{(1)}$, and $W_{(1)}$ across the whole of the inner region.

I. Evaluation of the boundary conditions satisfied by the outer potentials

The time evolution of the flow pattern in the vicinity of the island is described by the set of vorticity diffusion equations (93) and (96). These equations form a system that is third order in the temporal variable T, and twelfth order in the spatial variable Ω. It follows that in order to uniquely specify the flow at all times after an initial time t_0, it is necessary to have three temporal boundary conditions valid for all Ω at $t = t_0$, and 12 spatial boundary conditions valid for all $t > t_0$. The three temporal boundary conditions are just the initial values of $\bar{h}_{-}(\Omega)$, $\overline{F}(\Omega)$, and $\bar{F}(\Omega)$ at $t = t_0$. The 12 spatial boundary conditions are not quite as obvious, and can be divided into three main groups.

(1) Three boundary conditions applied in the limit as $\Omega \to -1$ which ensure that the flow is well-behaved at the O point.

(2) Six boundary conditions applied at $\Omega = 1$ which ensure that the flow is well-behaved at the separatrix.

(3) Three boundary conditions applied in the limit $\Omega \to \infty$ which ensure that the island solution matches smoothly onto the external solution.

1. The boundary conditions at the O point

Boundary conditions at the O point are applied to Eqs. (96) by requiring that only the physically acceptable asymptotic forms of the spatial diffusion operators are present for all $t \geqslant t_0$. (If the system is evolved from an initial steady state to a final steady state this requirement is perfectly reasonable.)

Consider the asymptotic forms of

$$\overline{\nabla}_\perp^4 \bar{f} = 0\tag{114}$$

in the limit $\Omega \to -1$. It follows from the Appendix that

$$\underset{\Omega \to -1}{\text{lt}}\ \overline{\nabla}_\perp^4 \bar{f} \to \left(\frac{3}{8}q^2\frac{\partial^4}{\partial q^4} + \frac{3}{2}q\frac{\partial^3}{\partial q^3} + \frac{3}{4}\frac{\partial^2}{\partial q^2}\right)\bar{f}(q-1),\tag{115}$$

where $q = 1 + \Omega$. It is clear from the above that $\bar{f}(q-1)$ has the form

$$\bar{f}(q-1) \simeq a_0 + a_1 q + a_2 q \ln q + a_3 \ln q\tag{116}$$

at small q, where $a_{0 \to 3}$ are independent constants. At small q, the radial distance r_c from the O point is of order $q^{1/2}$, and the circulation velocity v_c is proportional to $q^{1/2}(\partial \bar{f}/\partial q)$. Clearly, the last asymptotic form in (116) is unphysical since it implies $v_c \propto 1/r_c$. Thus, the first boundary condition applied at the O point is

$$a_3 = 0.\tag{117}$$

Consider, now, the asymptotic forms of

$$\breve{\nabla}_\perp^4 \overline{F} = 0\tag{118}$$

in the limit $\Omega \to -1$. It follows from the Appendix that

$$
\begin{aligned}
\underset{\Omega \to -1}{\text{lt}}\ \breve{\nabla}_\perp^4 \overline{F} \to 0.07405\Big(q^2\frac{\partial^4}{\partial q^4} &+ 4q\frac{\partial^3}{\partial q^3} + 2\frac{\partial^2}{\partial q^2} \\
&+ \frac{3.3761}{q}\frac{\partial}{\partial q} - \frac{1.2660}{q^2}\Big)\overline{F}(q-1),
\end{aligned}\tag{119}
$$

where $q = 1 + \Omega$. If a power-law solution

$$\overline{F}(q-1) = q^\sigma\tag{120}$$

is substituted into (118) and (119), then σ is found to satisfy the indicial equation

$$
\begin{aligned}
\sigma(\sigma - 1)(\sigma - 2)(\sigma - 3) &+ 4\sigma(\sigma - 1)(\sigma - 2) \\
&+ 2\sigma(\sigma - 1) + 3.3761\sigma - 1.2660 = 0.
\end{aligned}\tag{121}
$$

The roots of the above are

$$
\begin{aligned}
\sigma_\pm &\equiv (\sigma_1 \pm \sigma_2 i) = (1.354 \pm 1.211i), \\
\sigma_3 &= 0.395, \\
\sigma_4 &= -1.067.
\end{aligned}\tag{122}
$$

Thus, $\overline{F}(q-1)$ has the form

$$
\begin{aligned}
\overline{F}(q-1) = b_1 \cos(\sigma_2 \ln q)q^{\sigma_1} &+ b_2 \sin(\sigma_2 \ln q)q^{\sigma_1} \\
&+ b_3 q^{\sigma_3} + b_4 q^{\sigma_4}
\end{aligned}\tag{123}
$$

at small q, where $b_{1 \to 4}$ are independent constants. The last two asymptotic forms do not satisfy the necessary requirement (105b) for the flow pattern associated with $\overline{F}(\Omega)$ to be reasonable in the vicinity of the O point. Thus, the final two boundary conditions applied at the O point are

$$b_3 = b_4 = 0.\tag{124}$$

Note that the two acceptable asymptotic forms in (123) appear to oscillate infinitely fast as $q \to 0$; this is not a problem, however, because when $q \sim O(\lambda^2)$ the viscous boundary layer at $X = 0$ becomes as wide as the circular flux-surfaces surrounding the O point, thus the limiting form (123) is only valid for $q \geqslant O(\lambda^2)$.

2. The boundary conditions at the separatrix

Consider the asymptotic forms of $\overline{\nabla}_1^4 \overline{h}_- = 0$ in the limit $\Omega \to 1$. It follows from the Appendix that

$$\lim_{\Omega \to 1} \overline{\nabla}_1^4 \overline{h}_- \to \left(\hat{A}(q)\frac{\partial^4}{\partial q^4} + \hat{B}(q)\frac{\partial^3}{\partial q^3} + \hat{C}\frac{\partial^2}{\partial q^2} \right)\overline{h}_-(1+q), \quad (125)$$

where

$$\begin{aligned}
q &= \Omega - 1, \\
\hat{A}(q) &= A_1(1+q), \\
\hat{B}(q) &= 3A_0(1+q), \\
\hat{C} &= \tfrac{1}{4}.
\end{aligned} \quad (126)$$

Note that $\hat{A}(q)$ and $\hat{B}(q)$ only have a logarithmic dependence on q in the vicinity of $q = 0$. Assuming (as is reasonable) that the behavior of $\overline{h}_-(\Omega)$ in the vicinity of $\Omega = 1$ is dominated by the asymptotic forms of the spatial diffusion operator $\overline{\nabla}_1^4$, it follows from (125) and (126) that

$$\begin{aligned}
\overline{h}_-(1+q) \simeq{}& \overline{h}_-(1) + \overline{h}'_-(1)q \\
&+ \frac{1}{2}\overline{h}''_-(1)\left[q^2 - \left(\frac{\hat{C}}{12\hat{A}(q)}\right)q^4 + \cdots \right] \\
&+ \frac{1}{6}\overline{h}'''_-(1)\left[q^3 - \left(\frac{\hat{B}(q)}{4\hat{A}(q)}\right)q^4 + \cdots \right] \quad (127)
\end{aligned}$$

at small q. Here, $\overline{h}_-(1)$, $\overline{h}'_-(1)$, etc. are independent constants. Similarly, the most general power-law expansion of $\overline{f}(\Omega)$ in the vicinity of the separatrix is

$$\begin{aligned}
\overline{f}(1+q) \simeq{}& \overline{f}(1) + \overline{f}'(1)q + \frac{1}{2}\overline{f}''(1) \\
&\times \left[q^2 - \left(\frac{\hat{C}}{12\hat{A}(q)}\right)q^4 + \cdots \right] \\
&+ \frac{1}{6}\overline{f}'''(1)\left[q^3 - \left(\frac{\hat{B}(q)}{4\hat{A}(q)}\right)q^4 + \cdots \right], \quad (128)
\end{aligned}$$

where $\overline{f}(1)$, $\overline{f}'(1)$, etc. are independent constants.

Consider now the asymptotic forms of $\overline{\nabla}_1^4 \overline{F} = 0$ in the limit $\Omega \to 1$. From the Appendix

$$\begin{aligned}
\lim_{\Omega \to 1} \overline{\nabla}_1^4 \overline{F} \to{}& \left(\breve{A}(q)\frac{\partial^4}{\partial q^4} + \breve{B}(q)\frac{\partial^3}{\partial q^3} + \breve{C}(q)\frac{\partial^2}{\partial q^2} \right.\\
&\left. + \frac{\breve{D}(q)}{q}\frac{\partial}{\partial q} + \frac{\breve{E}(q)}{q^2} \right)\overline{F}(1+q), \quad (129)
\end{aligned}$$

where

$$\begin{aligned}
\breve{A}(q) &= C_4(1+q), \\
\breve{B}(q) &= C_3(1+q), \\
\breve{C}(q) &= C_2(1+q), \\
\breve{D}(q) &= qC_1(1+q), \\
\breve{E}(q) &= q^2 C_0(1+q).
\end{aligned} \quad (130)$$

Note that $\breve{A}(q)\cdots\breve{E}(q)$ only have a logarithmic dependence on q in the vicinity of $q = 0$. Assuming that the behavior of $\overline{F}(\Omega)$ in the vicinity of $\Omega = 1$ is dominated by the asymptotic forms of the spatial diffusion operator $\overline{\nabla}_1^4$, it follows from (129) and (130) that

$$\begin{aligned}
\overline{F}(1+q) \simeq{}& \overline{F}(1)\left[1 + \left(\frac{\breve{E}(q)}{2\breve{A}(q)}\right)q^2 \ln(-q) + \cdots \right] + \overline{F}'(1)\left[q - \left(\frac{\breve{E}(q) + \breve{D}(q)}{6\breve{A}(q)}\right)q^3\ln(-q) + \cdots \right] \\
&+ \frac{1}{2}\overline{F}''(1)\left[q^2 - \left(\frac{2\breve{C}(q) + 2\breve{D}(q) + \breve{E}(q)}{24\breve{A}(q)}\right)q^4 + \cdots \right] + \frac{1}{6}\overline{F}'''(1)\left[q^3 - \left(\frac{\breve{B}(q)}{4\breve{A}(q)}\right)q^4 + \cdots \right] \quad (131)
\end{aligned}$$

at small q, where $\overline{F}(1)$, $\overline{F}'(1)$, etc. are independent constants.

The first three boundary conditions applied at $\Omega = 1$ come simply from the requirement that the electric potential (i.e., $\mathcal{H}$) be continuous at the separatrix. Thus, from (89), (127), (128), and (131) it follows that

$$\overline{h}_-(1) = \overline{f}(1) = \overline{F}(1) = 0 \quad (132)$$

[cf. Eq. (90)].

Equations (107), (108), (109), (127), (128), and (131) imply that

$$\mathcal{H}_{(0)'-}(1 + \lambda p, \xi) = U(p,\xi) = \left[\lambda\overline{h}'_-(1)\overline{U}_{(1)}(p,\xi) + \tfrac{1}{2}\lambda^2\overline{h}''_-(1)\overline{U}_{(2)}(p,\xi) + \tfrac{1}{6}\lambda^3\overline{h}'''_-(1)\overline{U}_{(3)}(p,\xi) \right] + O(\lambda^4),$$

$$\begin{aligned}
\mathcal{H}_{(0)'+}(1 + \lambda p, \xi) = {}&V(p,\xi) + W(p,\xi) \\
={}& \left[\lambda\overline{f}'(1)\overline{V}_{(1)}(p,\xi) + \tfrac{1}{2}\lambda^2\overline{f}''(1)\overline{V}_{(2)}(p,\xi) + \tfrac{1}{6}\lambda^3\overline{f}'''(1)\overline{V}_{(3)}(p,\xi) \right] \\
&+ \left[\lambda\overline{F}'(1)\overline{W}_{(1)}(p,\xi) + \tfrac{1}{2}\lambda^2\overline{F}''(1)\overline{W}_{(2)}(p,\xi) + \tfrac{1}{6}\lambda^3\overline{F}'''(1)\overline{W}_{(3)}(p,\xi) \right. \\
&\left. + \tfrac{1}{2}\lambda^3\overline{F}'(1)\overline{W}_{(3)'}(p,\xi) \right] + O(\lambda^4) \quad (133)
\end{aligned}$$

close to the separatrix. The potentials $\overline{U}_{(n)}$ and $\overline{V}_{(n)}$ have the symmetry of $\cos\xi$, whereas the $\overline{W}_{(n)}$ have the symmetry of $\sin\xi$. The boundary conditions satisfied by the various potentials appearing in (133) are

$$\begin{aligned}
&\overline{U}_{(n)} \to 0 \quad \text{as } p \to -\infty, \quad \overline{U}_{(n)} \to p^n \quad \text{as } p \to +\infty, \\
&\overline{V}_{(n)} \to p^n \quad \text{as } p \to -\infty, \quad \overline{V}_{(n)} \to 0 \quad \text{as } p \to +\infty, \\
&\overline{W}_{(n)} \to \Theta(1 + \lambda p, \xi)p^n \quad \text{as } p \to -\infty, \quad \overline{W}_{(n)} \to 0 \quad \text{as } p \to +\infty, \\
&\overline{W}_{(3)'} \to \Theta(1 + \lambda p, \xi)\Upsilon(\lambda p)p^3 \quad \text{as } p \to -\infty, \quad \overline{W}_{(3)'} \to 0 \quad \text{as } p \to +\infty,
\end{aligned} \quad (134)$$

where

$$\Upsilon(q) = \left(\frac{\breve{E}(q) + \breve{D}(q)}{\breve{A}(q)} \right) \ln\left(\frac{1}{(-q)} \right). \tag{135}$$

After some manipulation the flux-surface average of σX times the vorticity evolution equation (81) yields

$$-\frac{8}{\lambda^4} \frac{1}{(\omega_v \tau_R)} \left(\frac{r_s}{w} \right) \left(\frac{1}{2} \right) \langle \breve{J}_+ \sin \xi \rangle$$

$$= \frac{1}{\lambda^2} \frac{\partial}{\partial T} \left[\frac{\partial}{\partial p} \left(\langle X^3 \frac{\partial U}{\partial p} \rangle - \frac{\lambda}{2} \langle XU \rangle \right) \right] - \frac{1}{\lambda^4} \left[\frac{\partial}{\partial p} \left(\langle X^5 \frac{\partial^3 U}{\partial p^3} \rangle + \lambda \langle X^3 \frac{\partial^2 U}{\partial p^2} \rangle - \frac{\lambda^2}{4} \langle X \frac{\partial U}{\partial p} \rangle \right) \right]$$

$$+ \frac{1}{\lambda^3} \left[\langle X^2 \left(\frac{\partial V}{\partial p} \frac{\partial}{\partial \xi} - \frac{\partial V}{\partial \xi} \frac{\partial}{\partial p} \right) \breve{\nabla}_1^2 W \rangle + \langle X^2 \left(\frac{\partial W}{\partial p} \frac{\partial}{\partial \xi} - \frac{\partial W}{\partial \xi} \frac{\partial}{\partial p} \right) \breve{\nabla}_1^2 V \rangle \right] \tag{136}$$

close to the separatrix, where

$$\breve{\nabla}_1^2 \equiv X^2 \frac{\partial^2}{\partial p^2} + \frac{\lambda}{2} \frac{\partial}{\partial p}. \tag{137}$$

In the derivation of Eq. (136) use has been made of (62), (107) and the symmetry properties of U, V and W. Similarly, the flux-surface average of $\sigma\Xi$ times Eq. (81) gives

$$\frac{8}{\lambda^4} \frac{1}{(\omega_v \tau_R)} \left(\frac{r_s}{w} \right) \left(\frac{1}{\sqrt{2}} \right) \langle \breve{J}_+ \cos \xi \rangle = \frac{1}{\lambda^3} \left[\langle X\Xi \left(\frac{\partial U}{\partial p} \frac{\partial}{\partial \xi} - \frac{\partial U}{\partial \xi} \frac{\partial}{\partial p} \right) \breve{\nabla}_1^2 U \rangle \right.$$

$$\left. + \langle X\Xi \left(\frac{\partial V}{\partial p} \frac{\partial}{\partial \xi} - \frac{\partial V}{\partial \xi} \frac{\partial}{\partial p} \right) \breve{\nabla}_1^2 V \rangle + \langle X\Xi \left(\frac{\partial W}{\partial p} \frac{\partial}{\partial \xi} - \frac{\partial W}{\partial \xi} \frac{\partial}{\partial p} \right) \breve{\nabla}_1^2 W \rangle \right], \tag{138}$$

where use has been made of (63). Next, the flux-surface average of (81) gives

$$\left(\frac{8}{\lambda^4} \right) \frac{1}{(\omega_v \tau_R)} \left(\frac{r_s}{w} \right) \frac{1}{2\pi} \left[J_- (2\pi - \xi_0) - J_- (\xi_0) \right]$$

$$= \frac{1}{\lambda^2} \frac{\partial}{\partial T} \left(\frac{\partial}{\partial p} \langle X^2 \frac{\partial V}{\partial p} \rangle \right) - \frac{1}{\lambda^4} \left[\frac{\partial}{\partial p} \left(\langle X^4 \frac{\partial^3 V}{\partial p^3} \rangle + \frac{3}{2} \lambda \langle X^2 \frac{\partial^2 V}{\partial p^2} \rangle \right) \right]$$

$$+ \frac{1}{\lambda^3} \left[\langle X \left(\frac{\partial U}{\partial p} \frac{\partial}{\partial \xi} - \frac{\partial U}{\partial \xi} \frac{\partial}{\partial p} \right) \breve{\nabla}_1^2 W \rangle + \langle X \left(\frac{\partial W}{\partial p} \frac{\partial}{\partial \xi} - \frac{\partial W}{\partial \xi} \frac{\partial}{\partial p} \right) \breve{\nabla}_1^2 U \rangle \right], \tag{139}$$

where use has been made of (57). Finally, the flux-surface average of Θ times (81) yields

$$\left(\frac{8}{\lambda^4} \right) \frac{1}{(\omega_v \tau_R)} \left(\frac{r_s}{w} \right) \left(\frac{1}{\sqrt{2}} \right) \left(\langle J_- \rangle - \frac{1}{2} \left[J_- (2\pi - \xi_0) + J_- (\xi_0) \right] \langle 1 \rangle \right)$$

$$= \frac{1}{\lambda^2} \frac{\partial}{\partial T} \left[\frac{\partial}{\partial p} \left(\langle \Theta X^2 \frac{\partial W}{\partial p} \rangle - \lambda \langle \Theta' X^2 W \rangle \right) + \lambda^2 \left(\langle \Theta'' X^2 W \rangle + \frac{1}{2} \langle \Theta' W \rangle \right) \right]$$

$$- \frac{1}{\lambda^4} \left\{ \frac{\partial}{\partial p} \left[\langle \Theta X^4 \frac{\partial^3 W}{\partial p^3} \rangle - \lambda \left(\langle \Theta' X^4 \frac{\partial^2 W}{\partial p^2} \rangle - \frac{3}{2} \langle \Theta X^2 \frac{\partial^2 W}{\partial p^2} \rangle \right) \right. \right.$$

$$\left. + \lambda^2 \left(\langle \Theta'' X^4 \frac{\partial W}{\partial p} \rangle \right) - \lambda^3 \left(\langle \Theta''' X^4 W \rangle + \frac{3}{2} \langle \Theta' X^2 W \rangle \right) \right] + \lambda^4 \left(\langle \Theta'''' X^4 W \rangle + 3 \langle \Theta''' X^2 W \rangle + \frac{3}{4} \langle \Theta'' W \rangle \right) \right\}$$

$$+ \frac{1}{\lambda^3} \left[\langle X\Theta \left(\frac{\partial U}{\partial p} \frac{\partial}{\partial \xi} - \frac{\partial U}{\partial \xi} \frac{\partial}{\partial p} \right) \breve{\nabla}_1^2 V \rangle + \langle X\Theta \left(\frac{\partial V}{\partial p} \frac{\partial}{\partial \xi} - \frac{\partial V}{\partial \xi} \frac{\partial}{\partial p} \right) \breve{\nabla}_1^2 U \rangle \right], \tag{140}$$

where $'$ denotes $\partial/\partial\Omega$, and use has been made of (61).

Now the boundary conditions applied at the separatrix must be such as to ensure that the flow in the region $\Omega > 1$ links up *smoothly* with the flow in the region $\Omega < 1$. In particular, if the resistive skin diffusion rate across a layer of thickness λ is much greater than any other real frequency in the system, i.e., if

$$(\omega \tau_R) \ll (r_s/w)^2 (1/\lambda^2) \tag{141}$$

(as is always likely to be the case if $\lambda \ll 1$), then the even current distribution J_+ must have no "spike" at $\Omega = 1$. In other words, the integral constraints (68) should not contain a contribution from what appears to be a sheet current on the separatrix. It is easily seen from the form of Eqs. (68), plus that of the vorticity evolution equation (81), that this requirement *implies*

$$\frac{8}{\lambda^4}\frac{1}{(\omega_v \tau_R)}\left(\frac{r_s}{w}\right)$$
$$\times \int_{1-\delta}^{1+\delta}\langle \tilde{J}_+ \sin\xi\rangle d\Omega \sim O(\delta) + O(\delta \ln\delta) + \cdots,$$

$$\frac{8}{\lambda^4}\frac{1}{(\omega_v \tau_R)}\left(\frac{r_s}{w}\right)$$
$$\times \int_{1-\delta}^{1+\delta}\langle \tilde{J}_+ \cos\xi\rangle d\Omega \sim O(\delta) + O(\delta \ln\delta) + \cdots,$$
$$(142)$$

where $1 \gg \delta \gg \lambda$. Equations (133), (134), (136), (138), and (142) can be combined to form the following two boundary conditions applicable at the separatrix:

$$0 = Z_3(1)\frac{\partial}{\partial T}\bar{h}\,'_-(1) - [Z_5(1)\bar{h}\,'''_-(1) + Z_3(1)\bar{h}\,''_-(1)$$
$$-\tfrac{1}{4}Z_1(1)\bar{h}\,'_-(1)] + \alpha_{VW}\bar{f}\,'5(1)\bar{F}'(1) + O(\delta)$$
$$+ O(\delta \ln\delta),$$
$$0 = \alpha_{UU}[\bar{h}\,'_-(1)]^2 + \alpha_{VV}[\bar{f}'(1)]^2 + \alpha_{WW}[\bar{F}'(1)]^2$$
$$+ O(\delta) + O(\delta \ln\delta), \qquad (143)$$

where the $Z_i(\Omega)$ are flux-surface average quantities evaluated in the Appendix. The various coupling coefficients are given by

$$\alpha_{VW} = \int_{-\delta/\lambda}^{\delta/\lambda}\left[\left\langle X^2\left(\frac{\partial\bar{V}_{(1)}}{\partial p}\frac{\partial}{\partial\xi} - \frac{\partial\bar{V}_{(1)}}{\partial\xi}\frac{\partial}{\partial p}\right)\check{\nabla}_\perp^2\overline{W}_{(1)}\right\rangle\right.$$
$$\left.+ \left\langle X^2\left(\frac{\partial\overline{W}_{(1)}}{\partial p}\frac{\partial}{\partial\xi} - \frac{\partial\overline{W}_{(1)}}{\partial\xi}\frac{\partial}{\partial p}\right)\check{\nabla}_\perp^2\bar{V}_{(1)}\right\rangle\right]dp,$$

$$\alpha_{UU} = \int_{-\delta/\lambda}^{\delta/\lambda}\left\langle X\Xi\left(\frac{\partial\overline{U}_{(1)}}{\partial p}\frac{\partial}{\partial\xi} - \frac{\partial\overline{U}_{(1)}}{\partial\xi}\frac{\partial}{\partial p}\right)\check{\nabla}_\perp^2\overline{U}_{(1)}\right\rangle dp,$$
$$(144)$$

$$\alpha_{VV} = \int_{-\delta/\lambda}^{\delta/\lambda}\left\langle X\Xi\left(\frac{\partial\bar{V}_{(1)}}{\partial p}\frac{\partial}{\partial\xi} - \frac{\partial\bar{V}_{(1)}}{\partial\xi}\frac{\partial}{\partial p}\right)\check{\nabla}_\perp^2\bar{V}_{(1)}\right\rangle dp,$$

$$\alpha_{WW} = \int_{-\delta/\lambda}^{\delta/\lambda}\left\langle X\Xi\left(\frac{\partial\overline{W}_{(1)}}{\partial p}\frac{\partial}{\partial\xi} - \frac{\partial\overline{W}_{(1)}}{\partial\xi}\frac{\partial}{\partial p}\right)\check{\nabla}_\perp^2\overline{W}_{(1)}\right\rangle dp.$$

The boundary conditions must also ensure that the odd current distribution J_- is well-behaved in the vicinity of the separatrix. In particular, in order to make sure that $\tilde{J}_{(1)-} \to 0$ as $X \to 0$, the left-hand side of Eq. (139) must be zero inside the viscous layer [it is obviously zero outside from Eqs. (97), (98), and symmetry]. The integral of (139) from $\Omega = 1 - \delta$ to $\Omega = 1 + \delta$ yields the final boundary condition applicable at the separatrix:

$$0 = Z_2(1)\frac{\partial}{\partial T}\bar{f}'(1) - \left(Z_4(1)\bar{f}'''(1) + \frac{3}{2}Z_2(1)\bar{f}''(1)\right)$$
$$- \alpha_{UW}\bar{h}\,'_-(1)\bar{F}'(1) + O(\delta) + O(\delta \ln\delta), \qquad (145)$$

where

$$\alpha_{UW} = \int_{-\delta/\lambda}^{\delta/\lambda}\left[\left\langle X\left(\frac{\partial\overline{U}_{(1)}}{\partial p}\frac{\partial}{\partial\xi} - \frac{\partial\overline{U}_{(1)}}{\partial\xi}\frac{\partial}{\partial p}\right)\check{\nabla}_\perp^2\overline{W}_{(1)}\right\rangle\right.$$
$$\left.+ \left\langle X\left(\frac{\partial\overline{W}_{(1)}}{\partial p}\frac{\partial}{\partial\xi} - \frac{\partial\overline{W}_{(1)}}{\partial\xi}\frac{\partial}{\partial p}\right)\check{\nabla}_\perp^2\overline{U}_{(1)}\right\rangle\right]dp.$$
$$(146)$$

Note that, in general, the left-hand side of Eq. (140) is non-zero inside the viscous layer [again, it is obviously zero outside from Eqs. (97) and (98)]. This is symptomatic of the fact that the expression for $J_{(0)-}$ given in Eq. (100) is not well-defined inside the layer. It follows that there is no fourth boundary condition at the separatrix associated with the integral of Eq. (140) across the layer.

Equations (143) and (145) [which effectively fix the relative values of $\bar{h}\,'_-(1)$, $\bar{f}'(1)$ and $\bar{F}'(1)$] describe how the various different types of flow are coupled together by advective inertia at the separatrix. The relative strengths of the different couplings are parametrized by the coupling coefficients α_{UW}, α_{VW}, α_{UU}, α_{VV}, and α_{WW}. Thus, α_{UW} measures the coupling of even flow outside the separatrix to convection-cell-type flow inside the separatrix, α_{UU} measures the self-coupling of even flow outside the separatrix, etc.

3. The boundary conditions at $\Omega \to \infty$

Consider the asymptotic forms of $\overline{\nabla}_\perp^4 \bar{h}_- = 0$ in the limit $\Omega \to \infty$. It follows from the Appendix that

$$\mathrm{lt}\,\Omega\to\infty\ \overline{\nabla}_\perp^4\bar{h}_- = 0$$
$$\to \left(\Omega^2\frac{\partial^4}{\partial\Omega^4} + 3\Omega\frac{\partial^3}{\partial\Omega^3} + \frac{3}{4}\frac{\partial^2}{\partial\Omega^2}\right)\bar{h}_-(\Omega) = 0.$$
$$(147)$$

Assuming (as is reasonable) that the behavior of $\bar{h}_-(\Omega)$ as $\Omega \to \infty$ is dominated by the asymptotic forms of the spatial diffusion operator $\overline{\nabla}_\perp^4$, it follows from (147) that

$$\bar{h}_-(\Omega) \simeq c_0 + c_1\Omega^{1/2} + c_2\Omega + c_3\Omega^{3/2} \qquad (148)$$

at large Ω, where c_{0-3} are independent constants. Comparing the above with the boundary condition (91) it becomes clear that

$$c_3 = 0, \qquad (149a)$$
$$c_2 = 0, \qquad (149b)$$
$$c_1 = (k_\theta u_{\mathrm{eq}} - \omega)/\omega_v. \qquad (149c)$$

Equations (149) comprise the three external boundary conditions.

Equations (117), (124), (132), (143), (145), and (149) make up the 12 spatial boundary conditions applied to the system of vorticity diffusion equations (93) and (96).

J. Evaluation of the coupling coefficients

Equations (144) and (146) can be integrated by parts to give

$$\alpha_{VW} = \int_{-\delta/\lambda}^{\delta/\lambda}\left[\left\langle X\left(\frac{\partial X}{\partial p}\frac{\partial\bar{V}_{(1)}}{\partial\xi} - \frac{\partial X}{\partial\xi}\frac{\partial\bar{V}_{(1)}}{\partial p}\right)\check{\nabla}_\perp^2\overline{W}_{(1)}\right\rangle\right.$$
$$\left.+ \left\langle X\left(\frac{\partial X}{\partial p}\frac{\partial\overline{W}_{(1)}}{\partial\xi} - \frac{\partial X}{\partial\xi}\frac{\partial\overline{W}_{(1)}}{\partial p}\right)\check{\nabla}_\perp^2\bar{V}_{(1)}\right\rangle\right]$$
$$\times dp + O(\delta),$$
$$(150)$$

$$\alpha_{UU} = \int_{-\delta/\lambda}^{\delta/\lambda}\left\langle X\left(\frac{\partial\Xi}{\partial p}\frac{\partial\overline{U}_{(1)}}{\partial\xi} - \frac{\partial\Xi}{\partial\xi}\frac{\partial\overline{U}_{(1)}}{\partial p}\right)\check{\nabla}_\perp^2\overline{U}_{(1)}\right\rangle dp,$$

$$\alpha_{VV} = \int_{-\delta/\lambda}^{\delta/\lambda} \left\langle X\left(\frac{\partial \Xi}{\partial p}\frac{\partial \overline{V}_{(1)}}{\partial \xi} - \frac{\partial \Xi}{\partial \xi}\frac{\partial \overline{V}_{(1)}}{\partial p}\right)\widetilde{\nabla}_1^2 \overline{V}_{(1)}\right\rangle dp,$$

$$\alpha_{WW} = \int_{-\delta/\lambda}^{\delta/\lambda} \left\langle X\left(\frac{\partial \Xi}{\partial p}\frac{\partial \overline{W}_{(1)}}{\partial \xi} - \frac{\partial \Xi}{\partial \xi}\frac{\partial \overline{W}_{(1)}}{\partial p}\right)\widetilde{\nabla}_1^2 \overline{W}_{(1)}\right\rangle$$
$$\times dp + O(\delta \ln \delta),$$

$$\alpha_{UW} = 0,$$

where use has been made of the symmetry properties of $\overline{U}_{(1)}$, $\overline{V}_{(1)}$, and $\overline{W}_{(1)}$. The above equations can be shown to reduce to

$$\alpha_{VW} = (1/3\sqrt{2})Z_3(1) + O(\delta), \tag{151a}$$

$$\alpha_{UU} = \tfrac{1}{2}A_3(1+\lambda) + \alpha_{UU(1)}, \tag{151b}$$

$$\alpha_{VV} = -\tfrac{1}{4}A_3(1+\lambda) + \alpha_{VV(1)}, \tag{151c}$$

$$\alpha_{WW} = -\tfrac{1}{4}A_{3'}(1+\lambda) + \alpha_{WW(1)}, \tag{151d}$$

$$\alpha_{UW} = 0, \tag{151e}$$

where use has been made of the asymptotic properties of $\overline{U}_{(1)}$, $\overline{V}_{(1)}$, and $\overline{W}_{(1)}$. The flux-surface average quantities $Z_3(\Omega)$, $A_3(\Omega)$, and $A_{3'}(\Omega)$ are evaluated in the Appendix. The residual coupling coefficients $\alpha_{UU(1)}$, $\alpha_{VV(1)}$, and $\alpha_{WW(1)}$ are $O[\ln(\lambda)]^{-2}$ and depend on the exact behavior

of $\overline{U}_{(1)}$, $\overline{V}_{(1)}$, and $\overline{W}_{(1)}$, respectively, in the inner region. Thus, without ever explicitly solving for $\overline{U}_{(1)}$, etc., we have obtained the values of the coupling coefficients accurate to $O[\ln(\lambda)]^{-1}$, which is sufficient for our purposes.

K. Derivation of the island evolution equations

At this stage, the only remaining unknowns in the system are the time derivatives of the island width, $w(t)$, and the island frequency, $\omega(t)$. These are determined, via Eqs. (68), by the first-order current distribution induced by the zero-order flow potentials $\bar{h}_-$, $\bar{f}$, and $\overline{F}$.

Equations (81), (89), (92), and (93) imply that

$$\left(\frac{8}{\lambda^4}\right)\frac{1}{(\omega_v \tau_R)}\left(\frac{r_s}{w}\right)X\frac{\partial \widetilde{J}_+}{\partial \xi}$$
$$= \frac{\partial}{\partial T}\widetilde{\nabla}_1^2 \bar{h}_- + X \sin \xi\, \bar{h}'_- \bar{h}''_- - \widetilde{\nabla}_1^4 \bar{h}_- \tag{152}$$

outside the separatrix, where

$$\widetilde{\nabla}_1^2 \equiv \widetilde{X}^2\frac{\partial^2}{\partial \Omega^2},$$

$$\widetilde{\nabla}_1^4 \equiv \widetilde{X}^4\frac{\partial^4}{\partial \Omega^4} + 3\widetilde{X}^2\frac{\partial^3}{\partial \Omega^3}. \tag{153}$$

Similarly,

$$\left(\frac{8}{\lambda^4}\right)\frac{1}{(\omega_v \tau_R)}\left(\frac{r_s}{w}\right)X\frac{\partial \widetilde{J}_+}{\partial \xi}$$

$$= X \sin \xi\, \bar{f}'\bar{f}'' + \left(-\frac{1}{2}\frac{1}{\sqrt{2}}\frac{\Theta'}{X^2} + \frac{3}{2}\frac{1}{\sqrt{2}}\Theta'' + \frac{1}{\sqrt{2}}X^2\Theta''' + X \sin \xi\, \Theta'\Theta''\right)\overline{F}^2$$

$$+ \left(-\frac{1}{2}\frac{1}{\sqrt{2}}\frac{\Theta}{X^2} + X \sin \xi\, \Theta\Theta'' + \frac{7}{2}\frac{1}{\sqrt{2}}\Theta' + 3\frac{1}{\sqrt{2}}X^2\Theta'' + 2X \sin \xi\, \Theta'\Theta'\right)\overline{F}\,\overline{F}'$$

$$+ \left(\frac{3}{2}\frac{1}{\sqrt{2}}\Theta + 2\frac{1}{\sqrt{2}}X^2\Theta' + X \sin \xi\, \Theta\Theta'\right)\overline{F}\,\overline{F}''$$

$$+ \frac{1}{\sqrt{2}}X^2\Theta\overline{F}\,\overline{F}''' + \left(\frac{1}{2}\frac{1}{\sqrt{2}}\Theta + 2X \sin \xi\, \Theta\Theta'\right)\overline{F}'^2 + \left(-\frac{1}{\sqrt{2}}X^2\Theta + X \sin \xi\, \Theta\Theta\right)\overline{F}'\overline{F}''$$

$$+ \left(-\frac{1}{2}\frac{1}{\sqrt{2}}\frac{1}{X^2} + X \sin \xi\, \Theta''\right)\bar{f}'\overline{F} + \left(\frac{1}{2}\frac{1}{\sqrt{2}} + 2X \sin \xi\, \Theta'\right)\bar{f}'\overline{F}'$$

$$+ \left(-\frac{1}{\sqrt{2}}X^2 + X \sin \xi\, \Theta\right)\bar{f}'\overline{F}'' + \left(\frac{3}{2}\frac{1}{\sqrt{2}} + X \sin \xi\, \Theta'\right)\bar{f}''\overline{F} + X \sin \xi\, \Theta\bar{f}''\overline{F}' + \frac{1}{\sqrt{2}}X^2\bar{f}'''\overline{F} \tag{154}$$

inside the separatrix, where $'$ denotes $\partial/\partial\Omega$.

With the aid of (62) and (63), Eqs. (68) reduce to

$$\int_{-1}^{\infty} d\Omega \langle \cos \xi\rangle \overline{J}_+ + \sqrt{2}\int_{-1}^{\infty} d\Omega \left\langle \Xi X\frac{\partial \widetilde{J}_+}{\partial \xi}\right\rangle = \frac{1}{4}\,\text{Re}(\Delta' r_s),$$

$$\int_{-1}^{\infty} d\Omega \left\langle X^2\frac{\partial \widetilde{J}_+}{\partial \xi}\right\rangle = \frac{1}{8}\,\text{Im}(\Delta' r_s). \tag{155}$$

Making use of (51), (75a), (82), (152), and (154), the island evolution equations can be shown to take the form

$$I_1 \tau_R \frac{d}{dt}\left(\frac{w}{r_s}\right) = \text{Re}(\Delta' r_s) - I_2(\omega_v \tau_H)^2\left(\frac{r_s}{w}\right)^3, \tag{156a}$$

$$\frac{\partial}{\partial T}I_3 - I_4 + \text{Im}(\Delta' r_s)(\omega_v \tau_H)^{-2}\left(\frac{w}{r_s}\right)^3 = 0, \tag{156b}$$

where

$$I_1 = 4 \int_{-1}^{\infty} A_2(\Omega) d\Omega,$$

$$I_2 = 32\sqrt{2} \int_{1}^{\infty} A_3(\Omega) \overline{h}'_- \overline{h}''_- d\Omega + 32\sqrt{2} \int_{-1}^{+1} [A_3(\Omega)\overline{f}'\overline{f}'' + D_0(\Omega)\overline{F}^2 + D_1(\Omega)\overline{F}\overline{F}' + D_2(\Omega)\overline{F}\overline{F}''$$

$$+ D_3(\Omega)\overline{F}'^2 + D_4(\Omega)\overline{F}\overline{F}''' + D_5(\Omega)\overline{F}'\overline{F}'']d\Omega,$$

$$I_3 = 64 \int_{1}^{\infty} \left[\left(\frac{A_0(\Omega)A_5(\Omega)}{A_1(\Omega)} - A_4(\Omega) \right) \overline{h}''_- + \frac{1}{2}\frac{A_5(\Omega)}{A_1(\Omega)} \overline{h}'_- \right] d\Omega,$$

$$I_4 = 64 \int_{1}^{\infty} \left[3\left(\frac{A_0(\Omega)A_5(\Omega)}{A_1(\Omega)} - A_4(\Omega) \right) \overline{h}'''_- + \frac{3}{4}\frac{A_5(\Omega)}{A_1(\Omega)} \overline{h}''_- \right] d\Omega$$

$$+ 64 \int_{-1}^{+1} [E_0(\Omega)\overline{f}'\overline{F} + E_1(\Omega)\overline{f}''\overline{F} + E_2(\Omega)\overline{f}'\overline{F}' + E_3(\Omega)\overline{f}'\overline{F}'' + E_4(\Omega)\overline{f}'''\overline{F} + E_5(\Omega)\overline{f}''\overline{F}']d\Omega. \quad (157)$$

Here, the $A_i(\Omega)$, $D_i(\Omega)$, and $E_i(\Omega)$ are flux-surface average quantities specified in the Appendix. Note that the boundary conditions (142) ensure that no surface terms from the separatrix appear in the above equations.

Equation (156a) describes the time evolution of the island width $w(t)$ in a fairly straightforward manner. The first term on the right-hand side is the usual Rutherford[16] term, the second (which is generally stabilizing) comes ultimately from the inertia associated with the various flow patterns induced around the island due to its motion relative to the equilibrium plasma. (In fact, the plasma inertia manifests itself via perpendicular polarization currents, which are required to maintain force balance across flux surfaces. Now perpendicular currents can give rise to parallel currents via $\nabla \cdot \mathbf{j} = 0$. It is these parallel currents that modify the poloidal field structure and, thus, affect the width of the island.) Equation (156b) describes the time evolution of the island frequency $\omega(t)$ in a rather indirect way, through the time evolution of the integral $I_3(t)$. Now, I_3 depends on the flow potential $\overline{h}_-(\Omega)$, which in turn depends on ω through the boundary condition (149c). The second term in this equation comes from the viscous drag exerted on the propagating island by the plasma, the third term is the usual nonlinear torque on the island due to external coil currents.[22]

The second term in Eq. (156b) describes the viscous drag exerted by the equilibrium plasma on the magnetic island. However, by Newton's third law of motion the magnetic island exerts an equal and opposite drag on the plasma. This drag tends to modify the equilibrium flow profile external to the island on a momentum confinement time scale $\tau_M \sim \omega_s^{-1}$. It follows that the quantity u_{eq}, appearing in the boundary condition (149c), evolves at a typical rate ω_s, which is much slower than the evolution rate of the island frequency ω, but possibly faster than that of the island width w. In the following, we neglect this effect for the sake of simplicity.

For the case of forced reconnection, the Δ' for the (m, n) mode is made up of two distinct components. The first component is the natural delta primed of the mode, Δ_0', which is assumed to be negative. The second component is due to the resonant magnetic perturbation applied to the edge of the plasma, at the forcing frequency Ω. Such a perturbation is most easily produced by allowing a current (I_c,

say) to flow around coils external to the plasma. It is easily demonstrated, using arguments similar to those employed in Sec. II B plus the definition of w, that

$$(\Delta' r_s) = (-\Delta_0' r_s)[(w_c/w)^2 e^{i[\varphi(t) - \Omega t]} - 1], \quad (158)$$

where w_c is the final island width obtained in a nonrotating plasma when the applied perturbation is completely resonant in frequency (i.e., when $\Omega = 0$). Note that $w_c \propto I_c^{1/2}$ to a good approximation.

L. The time-asymptotic steady-state solution

We have shown that the time evolution of the system is determined by the set of vorticity diffusion equations (93) and (96), subject to the (nonlinear) spatial boundary conditions (117), (124), (132), (143), (145), and (149), plus the two integral constraints (156). These equations comprise a rigorous theory for the interaction of resonant magnetic perturbations with rotating plasmas in cylindrical geometry. Unfortunately, in the full time-dependent problem the evolution of the island parameters w and ω, which is usually all that we wish to calculate, cannot be effectively decoupled from that of the flow pattern. Thus, in general, the only way to gain any useful information from the theory set out above is to solve a twelfth-order diffusion problem subject to nonlinear boundary conditions, and two rather complicated integral constraints. Fortunately, however, if we now restrict our attention to the time-asymptotic steady-state solution (assuming, of course, that such a solution exists) then the problem simplifies considerably.

It is clear from Eqs. (156) and (158) that a necessary condition for the flow pattern to be steady is

$$\varphi = \Omega t + \Delta\varphi,$$

$$\omega \equiv \frac{d\varphi}{dt} = \Omega; \quad (159)$$

i.e. the island must rotate at the forcing frequency Ω, but may have a nonzero phase shift $\Delta\varphi$ with respect to the applied perturbation at the edge of the plasma. (This type of behavior is similar to that obtained in Sec. II for the linear regime. There, in the final state, the induced perturbation at the rational surface was always found to rotate at the frequency Ω, but in general had a nonzero phase shift.)

Let

$$\bar{h}_-(\Omega) = -(\Omega'/\omega_v)\hat{h}(\Omega),$$

$$\bar{f}(\Omega) = -(\Omega'/\omega_v)[\bar{f}'(1)/\bar{h}'_-(1)]\hat{f}(\Omega), \qquad (160)$$

$$\bar{F}(\Omega) = -(\Omega'/\omega_v)[\bar{f}'(1)/\bar{h}'_-(1)]\hat{F}(\Omega),$$

where $\Omega' = \Omega - k_\theta u_{cq}$ is the Doppler-shifted forcing frequency seen in a frame rotating with the $\mathbf{E} \wedge \mathbf{B}$ velocity of the unperturbed plasma at the rational surface.

It follows from Eqs. (93), (148), (149), and (160), that in a steady state $\hat{h}(\Omega)$ satisfies

$$\bar{\nabla}_\perp^4 \hat{h} = 0 \qquad (161)$$

for $\Omega \geqslant 1$, subject to the boundary condition

$$\hat{h}(\Omega) \to \hat{c}_0 + \Omega^{1/2} \quad \text{as } \Omega \to \infty. \qquad (162)$$

The value of the unknown parameter $\hat{c}_0$ is determined by the application of the boundary condition

$$\hat{h}(1) = 0 \qquad (163)$$

[cf. Eq. (132)], where $\hat{h}(1)$ is obtained from the matching of $\hat{h}(\Omega)$ to the expansion (127) in the vicinity of the separatrix.

Similarly, in a steady state $\hat{f}(\Omega)$ satisfies

$$\bar{\nabla}_\perp^4 \hat{f} = 0 \qquad (164)$$

for $\Omega \leqslant 1$, subject to the boundary condition

$$\hat{f}(q-1) \to \hat{a}_0 + \hat{a}_1 q + \hat{a}_2 q \ln q \quad \text{as } q \to 0 \qquad (165)$$

[cf. Eqs. (96a), (116), and (117)]. The values of the unknown parameters $\hat{a}_0$, $\hat{a}_1$, and $\hat{a}_2$, are determined by the application of the boundary conditions

$$\hat{f}(1) = 0,$$
$$\hat{f}'(1) = \hat{h}'(1), \qquad (166)$$
$$[Z_4(1)/Z_2(1)]\hat{f}'''(1) + \tfrac{3}{2}\hat{f}''(1) = 0$$

[cf. Eqs. (132), (145), (151e), and (160)], where $\hat{f}(1)$, $\hat{f}'(1)$, etc. are obtained from the matching of $\hat{f}(\Omega)$ to the power-law expansion (128) in the vicinity of the separatrix.

Finally, in a steady state $\hat{F}(\Omega)$ satisfies

$$\bar{\nabla}_\perp^4 \hat{F} = 0 \qquad (167)$$

for $\Omega \leqslant 1$, subject to the boundary condition

$$\hat{F}(q-1) \to \hat{b}_1 \cos(\sigma_2 q) q^{\sigma_1} + \hat{b}_2 \sin(\sigma_2 q) q^{\sigma_1} \quad \text{as } q \to 0, \qquad (168)$$

where $\sigma_1 = 1.354$ and $\sigma_2 = 1.211$ [cf. Eqs. (96b), (122), (123), and (124)]. The values of the unknown parameters $\hat{b}_1$ and $\hat{b}_2$ are determined by the application of the boundary conditions

$$\hat{F}(1) = 0, \quad \hat{F}'(1) = \hat{h}'(1) \qquad (169)$$

[cf. Eqs. (132), and (160)], where $\hat{F}(1)$ and $\hat{F}'(1)$ are obtained by matching $\hat{F}(\Omega)$ to the power-law expansion (131) in the vicinity of the separatrix.

Figure 7 shows $\hat{h}(\Omega)$, $\hat{f}(\Omega)$, and $\hat{F}(\Omega)$, calculated in accordance with the scheme set out above. It can be seen that for a steady state the potential $\hat{f}(\Omega)$ has a particularly simple form, with $\hat{f} \propto (\Omega - 1)$ in the region $\Omega \leqslant 1$. This corresponds to a circulation velocity around flux surfaces inside the separatrix, which is everywhere proportional to $\nabla(\mathbf{k} \cdot \mathbf{B}/k)$.
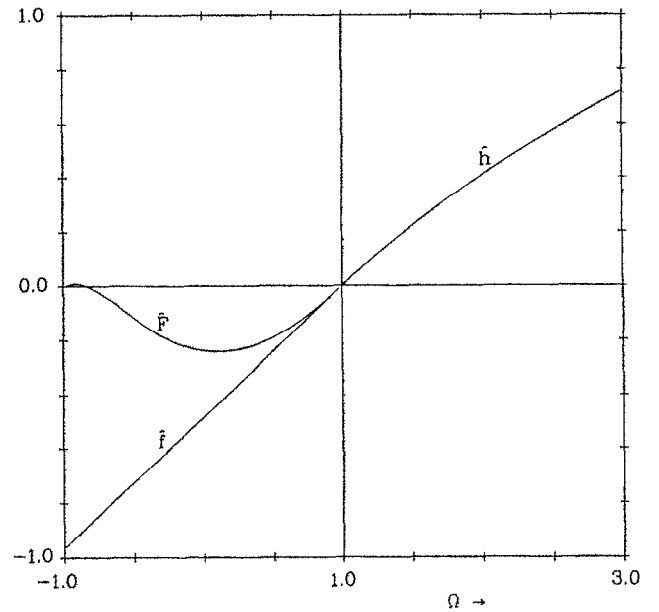

FIG. 7. The normalized steady-state potentials $\hat{h}(\Omega)$, $\hat{f}(\Omega)$, and $\hat{F}(\Omega)$, evaluated in accordance with the scheme set out toward the beginning of Sec. III L. Note that $\hat{f}(\Omega)$ is just a straight line (i.e., $\hat{f}''$, $\hat{f}'''$, etc. are zero).

In a steady state the nonlinear boundary conditions (143) imply

$$\bar{f}'(1)/\bar{h}'_-(1) = \pm [z_{NL}]^{1/2}, \qquad (170a)$$

$$\bar{F}'(1)/\bar{h}'_-(1) = \pm \alpha/[z_{NL}]^{1/2}, \qquad (170b)$$

$$z_{NL} = \tfrac{1}{2} + [\tfrac{1}{4} - \Gamma(\lambda)\alpha^2]^{1/2}, \qquad (170c)$$

$$\alpha = -(\omega_s/\Omega')(r_s/w)^2\beta, \qquad (170d)$$

$$\beta = 3\sqrt{2}\left(\frac{Z_5(1)}{Z_3(1)}\hat{h}'''(1) + \hat{h}''(1) - \frac{1}{4}\frac{Z_1(1)}{Z_3(1)}\hat{h}'(1)\right)$$
$$\times [\hat{h}'(1)]^{-2} = 0.099\,96, \qquad (170e)$$

$$\Gamma(\lambda) \simeq A_{3'}(1+\lambda)/A_3(1+\lambda), \qquad (170f)$$

where use has been made of Eqs. (151). The function $\Gamma(\lambda)$ is plotted in Fig. 8. The $\pm$ signs in Eqs. (170a) and (170b) correspond to two, otherwise physically indistinguishable, mirror-image flow patterns inside the separatrix. It can be shown, however, that when a small amount of equilibrium velocity shear is introduced into the problem, the state where the circulation around flux surfaces inside the separatrix *opposes* the imposed velocity shear gives rise to a slightly larger island than the state where the circulation enhances the equilibrium shear. Under normal circumstances we would expect the former to be the preferred state. Equation (170c) only has a physically acceptable (i.e., real and positive) solution when

$$\Gamma(\lambda)\alpha^2 < \tfrac{1}{4}. \qquad (171)$$

If the above inequality is violated then Eqs. (143) imply that $(\partial/\partial T)\bar{h}'_-(1)$ must be nonzero. Clearly, under these circumstances the assumption of a steady state is untenable. Note from Fig. 8 that the inequality (171) can always be
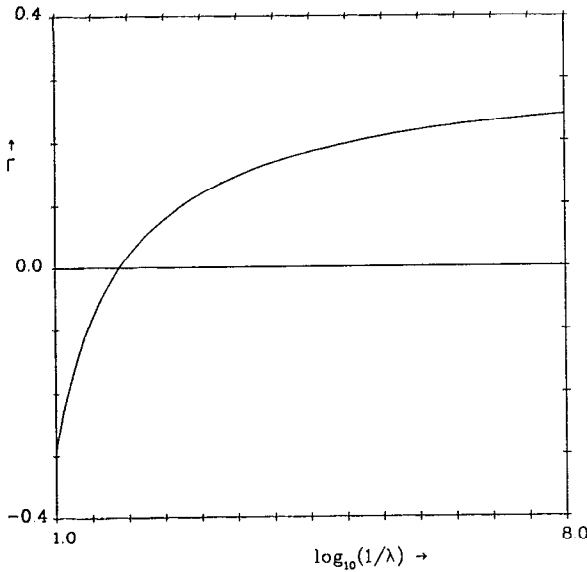
FIG. 8. The function Γ [cf. Eq. (170f)] plotted as a function of $\log_{10}(1/\lambda)$ [cf. Eq. (82a)]. Here, λ is approximately the width (in Ω) of the viscous layer at the separatrix. Note that $\Gamma < 0$ for relatively wide (i.e., $\lambda > 10^{-2}$) layers.

satisfied by increasing the layer width relative to the island width (i.e., by increasing λ).

In a steady state the island evolution equations (156) reduce to

$$I_1 \tau_R \frac{d}{dt}\left(\frac{w}{r_s}\right) = (-\Delta_0' r_s)\left[\cos \Delta\varphi \left(\frac{w_c}{w}\right)^2 - 1\right]$$

$$- \left(\frac{r_s}{w}\right)^3 (\Omega' \tau_H)^2 \left(I_{UU} + \frac{\alpha^2}{z_{NL}} I_{WW}\right),$$

$$\tag{172a}$$

$$\sin \Delta\varphi = -\left(\frac{r_s}{w}\right)^3 (\Omega' \omega_s \tau_H^2)\left(\frac{r_s}{w_c}\right)^2 \frac{(I_{U\Omega} + \beta I_{VW})}{(-\Delta_0' r_s)},$$

$$\tag{172b}$$

where

$$I_1 = 2.326,$$

$$I_{UU} = 32\sqrt{2} \int_1^\infty A_3 \bar{h}' \bar{h}'' \, d\Omega = 1.355,$$

$$I_{WW} = 32\sqrt{2} \int_{-1}^{+1} (D_0 \widehat{F}^2 + D_1 \widehat{FF}' + D_2 \widehat{FF}''$$

$$+ D_3 \widehat{F}'^2 + D_4 \widehat{FF}''' + D_5 \widehat{F}' \widehat{F}'') d\Omega = 0.8104,$$

$$I_{U\Omega} = 64 \int_1^\infty \left[3\left(\frac{A_0 A_5}{A_1} - A_4\right)\hat{h}''' + \frac{3}{4}\frac{A_5}{A_1}\hat{h}''\right] d\Omega$$

$$= 1.444, \tag{173}$$

$$I_{VW} = 64 \int_{-1}^{+1} (E_0 \hat{f}' \widehat{F} + E_1 \hat{f}'' \widehat{F} + E_2 \hat{f}' \widehat{F}'$$

$$+ E_3 \hat{f}' \widehat{F}'' + E_4 \hat{f}''' \widehat{F} + E_5 \hat{f}'' \widehat{F}') d\Omega = -2.412.$$

The d/dt term in Eq. (172a), which should strictly be dropped in a steady state, is retained merely to allow us to distinguish between stable and unstable solutions.

Equation (172a), which is the generalization of Eq. (33) for the case of a rotating plasma, describes how the inertia of even flow outside the separatrix (parametrized by the integral I_{UU}), and convection-cell type flow inside the separatrix (parametrized by the integral I_{WW}), both tend to *stabilize* a magnetic island which does not corotate with the local equilibrium plasma. The stabilizing effect increases with the square of the relative velocity of the island with respect to the local equilibrium plasma, but decreases as the cube of the island width. Note that in a steady state, flow circulating around flux surfaces inside the separatrix has no stabilizing effect on the island.

Equation (172b) describes how the viscous coupling between the island and the local equilibrium ion fluid gives rise to a phase shift between the island and the applied perturbation at the edge of the plasma. The integral $I_{U\Omega}$ parametrizes the viscous drag on the island due to the sheared ion flow outside the separatrix; this drag tends to shift the phase of the island *toward* the local equilibrium $E \wedge B$ frame which, in the absence of any ion diamagnetic effects, is identical to the frame of the local equilibrium ion fluid. The integral I_{VW} parametrizes the drag on the island due to the inertial interaction of circulatory and convection-cell flows inside the separatrix; this drag tends to shift the phase of the island *away* from the local $E \wedge B$ frame, but is much smaller in magnitude than the external drag. The nonlinear torque exerted on the island by the external coil currents increases as the cube of the island width and naturally tends to oppose the setting up of any nonzero phase shift; this accounts for the strong inverse dependence of $\Delta\varphi$ on w apparent in Eq. (172b). It is also clear from this equation that the viscous drag is proportional to the relative velocity of the island with respect to the local equilibrium ion fluid, and inversely proportional to the momentum confinement time scale $\tau_M \sim \omega_s^{-1}$. If the viscous drag on the island is weak [i.e., if the magnitude of the right-hand side of (172b) is much less than unity] then the phase shift is small. However, as the drag is increased (e.g., by a reduction in the momentum confinement time scale, a decrease in the island width, or an increase in the relative velocity of the island) a gradually increasing phase shift is set up. Naturally, the maximum possible phase shift that can be achieved is $\pi/2$. Once the viscous drag exceeds the critical value required to set up this phase shift [i.e., the magnitude of the right-hand side of (172b) becomes greater than unity] the *frequency* of the magnetic island starts to be dragged toward that of the local $E \wedge B$ frame (i.e., ω'/Ω' becomes less than unity). Under these circumstances the assumption of a steady state becomes untenable.

Equations (172) can be normalized to give

$$\frac{d}{dt}(W^4) \propto W(1 - \zeta_v^2 \zeta_\Omega^2/W^6)^{1/2} - W^3 - \zeta_\Omega, \tag{174a}$$

$$\sin \Delta\varphi = -\zeta_v \zeta_\Omega/W^3, \tag{174b}$$

where

$$W = w/w_c,$$

$$\zeta_\Omega = \frac{(\Omega' \tau_H)^2}{(w_c/r_s)^3} \frac{[I_{UU} + (\alpha^2/z_{NL})I_{WW}]}{(-\Delta_0' r_s)}, \tag{175}$$

$$\zeta_v = \left(\frac{w_s}{\Omega'}\right)\left(\frac{r_s}{w_c}\right)^2 \frac{(I_{UU} + \beta I_{VW})}{[I_{UU} + (\alpha^2/z_{NL})I_{WW}]}.$$

The parameter ζ_Ω is a measure of the relative velocity of the magnetic island with respect to the local equilibrium plasma. The parameter ζ_v is a measure of the viscous drag exerted by the plasma on the island. Note that ζ_Ω and ζ_v only have a fairly weak dependence on the island width through the w dependence of (α^2/z_{NL}).

The roots of (174a) can be calculated numerically. In the limit where rotation effects are negligible (i.e., $\zeta_\Omega \ll 1$) there are two equilibrium solutions; the first, denoted W_+, has $W_+ = 1$ (corresponding to full reconnection) with zero associated phase shift, and is stable; the second, denoted W_-, has $W_- \to 0$, with a $\pi/2$ associated phase shift, and is unstable. As rotation effects gradually become more important [i.e., as $\zeta_\Omega \to O(1)$] the stable root W_+ decreases monotonically from unity, while its associated phase shift increases monotonically from zero. Similarly, the unstable root W_- increases monotonically from zero, while its associated phase shift decreases monotonically from $\pi/2$. Eventually, at a critical value of the rotation parameter denoted $(\zeta_\Omega)_{max}$, the two roots coalesce. There are no steady-state solutions whatsoever for $\zeta_\Omega > (\zeta_\Omega)_{max}$, so the value of W_+ at $\zeta_\Omega = (\zeta_\omega)_{max}$, denoted $(W_+)_{min}$, is the minimum value of W achievable in a steady state at the particular ζ_v under consideration. Likewise, the phase shift of the stable solution at $\zeta_\Omega = (\zeta_\Omega)_{max}$, denoted $(\Delta\varphi)_{max}$, is the maximum-achievable phase shift at that ζ_v.

Table I shows values of W_+, W_-, and the associated phase shifts, calculated for various values of ζ_Ω, with $\zeta_v = 1.0$, and illustrates the behavior described in the preceding paragraph. Table II shows values of $(\zeta_\Omega)_{max}$, $(W_+)_{min}$, and $(\Delta\varphi)_{max}$, calculated for various values of ζ_v. It can be seen that as the viscous drag on the island increases (i.e., as ζ_v increases) the maximum value of ζ_Ω that is compatible with a steady state decreases, while the minimum allowable value of W, and the maximum allowable phase shift, both increase. Note that there are no stable steady-state solutions for which the island size w is less than 0.5774 of its

TABLE I. Steady-state solutions of the island evolution equations [Eqs. (174)] calculated for $\zeta_v = 1.0$. Here, W_+ and W_- are the normalized island widths (unity being equivalent to full reconnection) associated with the stable and unstable solutions, respectively. The quantities $\Delta\varphi_+$ and $\Delta\varphi_-$ are island phase shifts associated with the two solutions. As the rotation parameter ζ_Ω is increased the two solutions gradually approach one another, until at a critical value $[(\zeta_\Omega)_{max}]$ they coalesce. There are no steady-state solutions for $\zeta_\Omega > (\zeta_\Omega)_{max}$.

ζ_Ω	W_-	W_+	$-\Delta\varphi_-$	$-\Delta\varphi_+$
0.0000	0.0000	1.0000	90.0°	0.0°
0.0500	0.3732	0.9732	74.1°	3.1°
0.1000	0.4810	0.9416	64.0°	6.9°
0.1500	0.5703	0.9013	54.0°	11.8°
0.2000	0.6703	0.8375	41.6°	19.9°
0.2193	0.7598	0.7598	30.0°	30.0°

TABLE II. Steady-state solutions of the island evolution equations. The quantity $(\zeta_\Omega)_{max}$ is the maximum value of the rotation parameter compatible with a steady state for a given value of the viscosity parameter ζ_v; $(W_+)_{min}$ and $(-\Delta\varphi)_{max}$ are the associated (normalized) island width and phase shift, respectively. The quantity W_{crit} is the maximum possible island width associated with a nonsteady solution.

ζ_v	$(\zeta_\Omega)_{max}$	$(W_+)_{min}$	$(-\Delta\varphi)_{max}$	W_{crit}
0.0	0.3849	0.5774	0.0°	0.0000
0.1	0.3749	0.5992	10.0°	0.3347
0.5	0.2910	0.7035	24.7°	0.5260
1.0	0.2193	0.7598	30.0°	0.6030
1.5	0.1753	0.7886	32.4°.	0.6410
2.0	0.1458	0.8062	33.8°	0.6631
5.0	0.0724	0.8456	36.8°	0.7123
10.0	0.0394	0.8612	38.0°	0.7331
20.0	0.0206	0.8707	38.6°	0.7441

fully reconnected value w_c. Likewise, there are no stable steady states when the rotation parameter ζ_Ω exceeds the value 0.3849.

Consider the situation where ζ_Ω just exceeds the critical value $(\zeta_\Omega)_{max}$. Clearly, in the absence of a steady-state solution the system must find an acceptable time-varying solution. Although we can only conjecture as to what the properties of such a solution are likely to be, it seems clear that the island width must fall to a value which is, at least, small enough to enable viscosity to drag the island frequency ω off the forcing frequency Ω; from Eq.(174b) this implies $W < W_{crit} = [\zeta_v(\zeta_\Omega)_{max}]^{1/3}$ for a time-dependent solution. Values of W_{crit} calculated for various values of ζ_v are given in Table II. Note that W_{crit} is always less than $(W_+)_{min}$. This implies that, for any given ζ_v, there is a range of island widths, separating the steady-state from the non-steady-state solutions, which is inaccessible to the system. The upper limit of this forbidden range lies at $(W_+)_{min}$, while the lower limit lies somewhere below W_{crit}.

Suppose now that the system parameters (i.e., Ω, I_c) are varied adiabatically in such a manner as to increase ζ_Ω from a value just below the threshold value $(\zeta_\Omega)_{max}$, to a value just above it. It is clear from the above discussion that as ζ_Ω exceeds its threshold value the nature of the island solution will change discontinuously from a steady state to a non-steady state. This discontinuous behavior will be characterized by a sudden drop in the island width W, from a value $(W_+)_{min}$ to a value somewhat below W_{crit}. Table II implies that at relatively low viscosity ($\zeta_v \ll 1$) the drop in W is quite dramatic, but is fairly moderate at higher values of the viscosity ($\zeta_v \sim 1$). Note that even at very high values of the viscosity ($\zeta_v \gg 1$) the drop in W is non-negligible. Naturally, if the system parameters are varied in such a manner as to decrease ζ_Ω from a value just above the threshold $(\zeta_\Omega)_{max}$, to a value just below it, we would expect a sudden rise in the island width.

A comparison of Eq. (170c) and the definition of ζ_v indicates that at relatively low viscosity ($\zeta_v \ll 1$) the flow inside the separatrix is predominantly circulation around flux surfaces (i.e., $\alpha \ll 1$), but at higher values of the viscosity

R. Fitzpatrick and T. C. Hender   666

$[\zeta_v \sim O(1)]$ convection-cell type flow becomes significant [i.e., $\alpha \sim O(1)$]. Note from Eq. (171) that, under certain circumstances [i.e., $\Gamma(\lambda) > 0$], there may be a moderate upper limit on the value of ζ_v which is compatible with a steady state.

M. Discussion

We have derived a rigorous theory (in cylindrical geometry) describing the interaction of a moderate to large magnetic island, in a rotating plasma, with an externally applied resonant magnetic perturbation. This theory is particularly well suited to the interpretation of data from magnetic feedback experiments on MHD modes, but is also capable of shedding light on the eventual locking of such modes onto residual error fields. The equations determining the general time-dependent situation are extremely complex because, in this case, it is necessary to follow the time evolution of the flow pattern surrounding the propagating magnetic island in tandem with that of the island width and phase. The complete solution of these equations would be a very time consuming task, and would inevitably entail the writing of a large and sophisticated computer code. We hope to present the full solution at some future date, but, for the moment, we concentrate on a relatively simple (but still interesting) situation that can be dealt with analytically.

Suppose a resonant (m, n) magnetic perturbation, oscillating at some *constant* frequency Ω, is applied to the edge of a tokamak plasma. This situation is particularly relevant to those MHD feedback experiments where the coils are external to the vacuum vessel. In fact, in such experiments the applied signal is usually static (i.e., $\Omega = 0$).[1,3] After allowing a sufficient time for transients to die away, we would generally expect to observe a steady magnetic island on the (m, n) rational surface, rotating at the applied frequency Ω. Our theory enables us to calculate the properties of such islands (i.e., their width, and phase relative to that of the applied signal) in a fairly straightforward manner (see Sec. III L). It turns out that there are only two important parameters; firstly, $\zeta_\Omega \sim (\Omega'\tau_H)^2/(w_c/r_s)^3$, which measures the relative importance of rotation, and, secondly, $\zeta_v \sim 1/[(\Omega'\tau_M)(w_c/r_s)^2]$, which measures the relative importance of ion perpendicular viscosity. Here, Ω' is the Doppler-shifted applied frequency as seen in the local equilibrium $\mathbf{E} \wedge \mathbf{B}$ frame at the mode rational surface (radius r_s), w_c is the final island width that the applied signal would give rise to in the absence of rotation effects (N.B., $w_c \propto I_c^{1/2}$, where I_c is the coil current), τ_H is the local hydromagnetic time scale, and τ_M is the local momentum confinement time scale. At small values of the rotation and viscosity [i.e., ζ_Ω, $\zeta_v \ll 1$] the final island is fully reconnected (i.e., $w = w_c$) with zero phase shift. If the viscosity is non-negligible [i.e., $\zeta_v \sim O(1)$], the phase of the magnetic island is dragged somewhat in the direction of the local $\mathbf{E} \wedge \mathbf{B}$ frame, giving rise to a phase shift relative to the applied signal. This phase shift increases monotonically with increasing ζ_v. [Note, however, from Table II, that the phase shift never exceeds about 40°, even at very high viscosity (i.e., $\zeta_v \gg 1$).] As rotation gradually becomes significant [i.e., $\zeta_\Omega \to O(1)$] the final magnetic island is *stabilized* and only partially recon-

nects (i.e., $w < w_c$). Note that, at constant ζ_v, the island phase shift increases monotonically with increasing ζ_Ω. It turns out that there exists a threshold ζ_Ω, beyond which it is impossible to find a steady-state island solution; this threshold is $\zeta_\Omega \sim O(1)$ at low viscosity, but tends to be much less than unity at high viscosity (see Table II). As the rotation threshold is exceeded there is a sudden transition to a final nonsteady island (such islands, characteristically, do not rotate at the applied frequency Ω), accompanied by a sudden drop in the final island width. At low viscosity, this drop in the island width is quite substantial (e.g., an order of magnitude). If rotation is dominant (i.e., $\zeta_\Omega \gg 1$), then the system will not be able to achieve a final steady state; we conjecture, by analogy with the linear results presented in Sec. II, that in this situation reconnection will be very strongly inhibited (i.e., $w \ll w_c$).

IV. NUMERICAL RESULTS

In this section we present numerical simulations relating to the penetration of an $m = 2, n = 1$ applied helical field into a rotating plasma. These results will be shown to confirm the analytic predictions made in the preceding sections.

For the purpose of these simulations the following set of simple reduced MHD equations[23] is used:

$$\frac{\partial \psi}{\partial t} = -\mathbf{V}_\perp \cdot \nabla \psi - \frac{\partial \Phi}{\partial \zeta} + \frac{1}{S_\eta}(\eta J_\zeta - E_0) \qquad (176)$$

and

$$\frac{\partial U}{\partial t} = -\mathbf{V}_\perp \cdot \nabla U + (\nabla \psi \times \zeta) \cdot \nabla J_\zeta$$
$$- \frac{\partial J_\zeta}{\partial \zeta} + \nu \nabla_\perp^2 (U - U_{\text{eq}}), \qquad (177)$$

with $U = \nabla_\perp^2 \Phi$, $J_\zeta = \nabla_\perp^2 \psi$, $\mathbf{V}_\perp = \nabla \Phi \times \zeta$, and E_0 a constant electric field. In these equations the magnetic field is normalized to the constant toroidal magnetic field (B_ζ), all lengths are normalized to the minor radius (a), and time is normalized to the poloidal Alfvén time $\tau_A = R\sqrt{4\pi\rho_0}/B_\zeta$. Here, ρ_0 is the mass density, which is assumed to be uniform for the sake of simplicity. Note that the normalized magnetic field takes the form $\mathbf{B} = \zeta - (a/R)\nabla\psi \times \zeta$. The quantity η is the parallel electrical resistivity normalized with respect to the value on the magnetic axis (η_0), $\nu = \nu_\perp \tau_A/a^2$ is the normalized coefficient of perpendicular viscosity, and $S_\eta = \tau_\eta/\tau_A$ is the magnetic Reynolds number (as defined for these numerical calculations), with $\tau_\eta = 4\pi a^2/c^2\eta_0$. Diamagnetic effects have been neglected in Eqs. (176) and (177) for the sake of simplicity. It can easily be demonstrated that the above equations reduce to Eqs. (42) in the vicinity of the (m, n) mode rational surface.

When appropriate, an initial poloidal velocity profile is introduced by setting

$$\Phi_{\text{eq}} = \Phi_0[(r^2/2) - (r^4/4)], \qquad (178)$$

with $U_{\text{eq}} = \nabla_\perp^2 \Phi_{\text{eq}}$. From Eq. (177) it can be seen that the viscosity acts so as to relax the equilibrium velocity back to this initial profile.

For the (m, n) harmonic, the magnetic flux boundary

condition applied at the outer boundary ($r = 1$) is

$$\frac{\partial \psi_{m,n}}{\partial r} + \frac{m}{r} \psi_{m,n} = I_{c_{m,n}} e^{i\Omega_c t}. \qquad (179)$$

Equation (179) is consistent with the presence of helical sheet currents $I_{c_{m,n}}$ on the plasma boundary [representing the external conductor(s)], with an infinite vacuum region beyond. For the calculations presented here only the $m = 2$, $n = 1$ component of I_c is nonzero, so we shall omit the m, n subscript from now on. When appropriate, a real frequency Ω_c is applied to the "coils," this being completely equivalent to a uniform rigid toroidal rotation of the plasma with angular frequency $-\Omega_c$.

Equations (176) and (177) and the associated boundary conditions are discretized with a finite difference representation in the radial (r) direction, and a Fourier representation in the poloidal (θ) and toroidal (ζ) angles. Since rotational effects are included, both sine and cosine terms are required in these Fourier series. The temporal differencing is a semi-implicit scheme with the resistive and viscous terms included implicitly.[24]

We start by comparing the linear predictions of Sec. II with simulation results. For this comparison we use the profile $q(r) = 0.65(1 + 3r^2)$, with $S_\eta = 4 \times 10^5$ and $\nu = 0$. The equilibrium is found to be tearing stable with $\Delta_{2,1} = -1.05$. In this case, the relative rotation between the coils and plasma is achieved by rigid toroidal rotation of the plasma ($\Omega_c \neq 0$). The reconnected flux as a function of the plasma rotation, calculated from linear $m = 2$, $n = 1$ simulations, is compared with the analytic result [Eq. (17)] in Fig. 9. Considering the relatively low S_η (a restriction due to the long reconnection times), the agreement between numerical and analytic results is reasonably good.

We have also reproduced the main effects predicted by the nonlinear analytic theory. Figure 10 shows the $m = 2$,
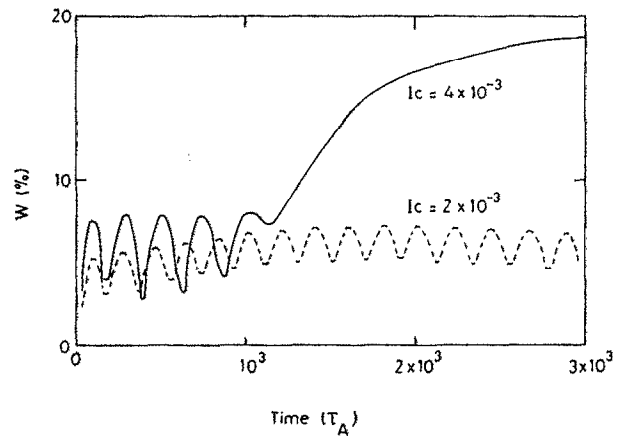
FIG. 10. The time evolution of the $m = 2$, $n = 1$ island width (W) for two applied helical "coil" currents (I_c). Here, $q = 0.7(1 + 2.75r^2)$, $S_\eta = 10^5$, and an equilibrium poloidal flow $\Phi_0 = 3 \times 10^{-2}$ is used.

$n = 1$ island width evolution, from nonlinear single helicity ($m/n = 2$) simulations, for two currents ($I_c = 2 \times 10^{-3}$ and 4×10^{-3}). Here $S_\eta = 10^5$, $\nu = 10^{-6}$, $q(r) = 0.7(1 + 2.75r^2)$, and an equilibrium poloidal flow $\Phi_0 = 3 \times 10^{-2}$ is used (with $\Omega_c = 0$). The equilibrium is again tearing stable with $\Delta_{2,1} = -0.71$. From Fig. 10 it can be seen that the lower current case ($I_c = 2 \times 10^{-3}$) does not reach a steady state, whereas the higher current case ($I_c = 4 \times 10^{-3}$) certainly does. This is precisely the behavior described in Sec. III L, where a threshold requirement for a steady-state solution is analytically predicted. In fact, for the parameters used in this simulation (Fig. 10) the analytic theory predicts a critical coil current for steady-state solutions in the range $I_c = 3-4 \times 10^{-3}$ with an associated critical island width $W = 2\sqrt{2}w \sim 10\%$ (of the minor radius), which is in good agreement with the simulations. Comparison with nonlinear simulations for the case of zero equilibrium flow shows that the higher current case ($I_c = 4 \times 10^{-3}$) reaches essentially full reconnection, whereas the lower current case ($I_c = 2 \times 10^{-3}$) only reaches $\sim 44\%$ reconnection. Thus, there is significant suppression of magnetic tearing when a steady state is not attained. Calculations for intermediate currents (I_c) indicate a threshold for steady state $I_c \sim 3 \times 10^{-3}$. In the vicinity of this threshold relatively small changes in the current ($I_c = 3 \times 10^{-3}$ to 4×10^{-3}) are observed to cause fairly large changes in the final island width ($W \sim 7.5\%$ to 19%). This sharp threshold corresponds to the point at which torque from the helical coils is sufficient to bring the equilibrium ($m = n = 0$) poloidal flow to rest. Figure 11 shows the final equilibrium poloidal velocity profiles corresponding to the cases shown in Fig. 10. It can be seen in the higher current case ($I_c = 4 \times 10^{-3}$) that the average poloidal flow is essentially zero within the island, whereas in the non-steady-state case ($I_c = 2 \times 10^{-3}$) the average velocity is only slightly reduced. We interpret these observations as follows: in the first case, the final rotation frequency of the magnetic island is identical with that of the externally applied coil current (i.e., zero), whereas in the
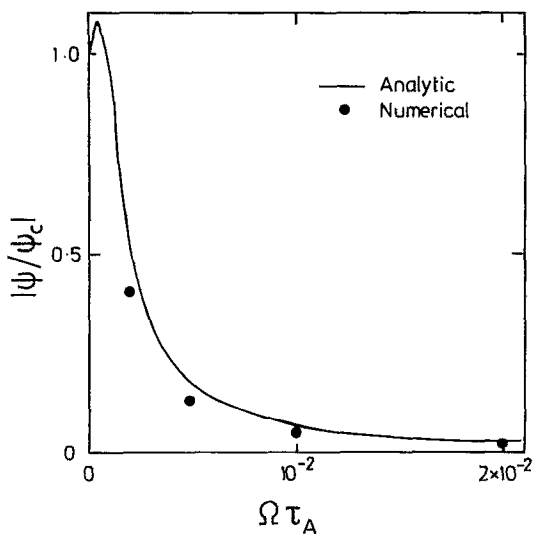

FIG. 9. The $m = 2$, $n = 1$ reconnected flux at $q = 2$ (normalized to that in the absence of rotation) versus the relative plasma-coil rotation frequency. The solid line is from the analytic theory [Eq. (17)] while the "dots" are from linear simulations. Here, $q = 0.65(1 + 3r^2)$ and $S_\eta = 4 \times 10^5$.
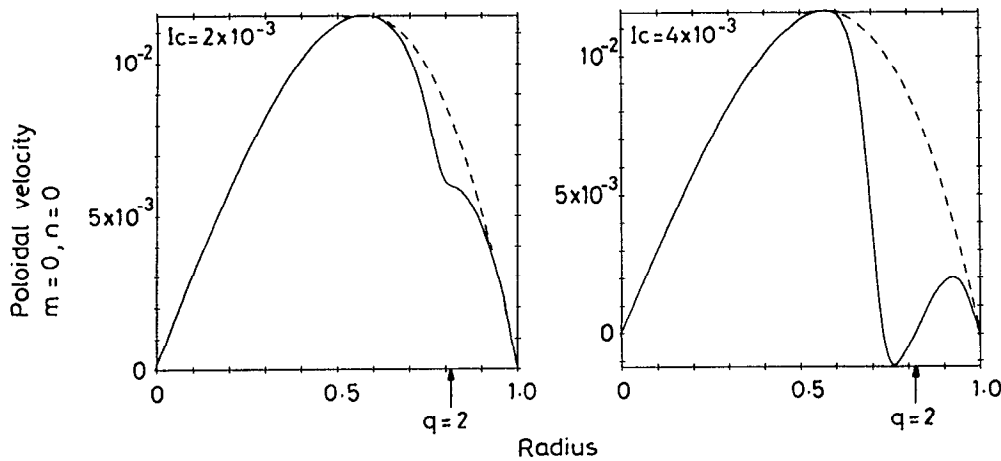
FIG. 11. Initial (broken lines) and final (solid lines) $m = n = 0$ poloidal velocity profiles corresponding to the two cases ($I_c = 2 \times 10^{-3}$ and 4×10^{-3}) shown in Fig. 10. The position of the $q = 2$ surface is indicated in both diagrams.

second case the island frequency is merely dragged slightly in the direction of the imposed coil frequency. This type of behavior is in accordance with the predictions of Sec. III L. Note, finally, that Fig. 11(b) shows clearly the presence of circulatory flow around flux-surfaces, inside the separatrix, which acts so as to *oppose* the equilibrium velocity shear across the island [this can be deduced from the fact that the (0,0) velocity becomes slightly negative just to the *left* of the O point]. This behavior is again in accordance with the predictions of Sec. III L.

V. CONCLUSIONS

In the preceding sections we have carried out a detailed investigation into the interaction of plasma rotation and magnetic reconnection in tokamaks. In the process, we have had to develop theories describing the penetration of a helical magnetic perturbation into a rotating plasma in both the linear and nonlinear regimes. The linear theory (see Sec. II) is a fairly straightforward extension of previously published work.[8] On the other hand, the nonlinear theory (see Sec. III) is quite novel, and is described briefly in the following paragraph.

We find that outside the island separatrix the plasma is constrained to flow around the perturbed magnetic flux surfaces, whereas inside the separatrix the flow is made up of a combination of circulation around flux surfaces and a convection-cell type pattern [cf. Eq. (89) and Fig. 6]. The flow in the vicinity of the island is ultimately driven by the relative motion of the island with respect to the local equilibrium plasma. We obtain vorticity evolution equations describing the viscous decay of the various permitted flow patterns [Eqs. (93) and (96)]. It turns out that a thin viscous boundary layer is required to link the flow smoothly on either side of the island separatrix. We obtain expressions describing the couplings of the various different types of flow at the separatrix due to the action of advective inertia in this layer [Eqs. (143) and (145)]. To lowest order the various coupling coefficients are found to be independent of the exact form of the boundary layer solution [cf. Eqs. (151)]. The flow in the vicinity of the magnetic island induces circulating currents. These currents can be integrated across flux sur-

faces to yield the equations governing the time evolution of the island width and frequency [Eqs. (156)]. In addition to the usual Rutherford[16] term our island width evolution equation contains a *stabilizing* term due ultimately to the inertia of the plasma flow patterns set up around the propagating island. This term is proportional to the square of the relative velocity of the island with respect to the local equilibrium plasma, and inversely proportional to the cube of the island width. The island frequency is found to depend on the relative strengths of the nonlinear torque due to currents flowing in external conductors, which attempts to make the island rotate at the imposed frequency, and the viscous coupling with the plasma, which attempts to make the island co-rotate with the local equilibrium flow.

The nonlinear theory outlined above is capable of modeling magnetic feedback stabilization, mode locking by error fields, and, ultimately, toroidal coupling of islands of neighboring rational surfaces. These are all topics of considerable interest to experimentalists. As an illustrative example, in Sec. III L, we use the theory to predict the properties of the final steady-state island induced when a helical magnetic perturbation is applied to a tearing-stable tokamak plasma equilibrium.

The major conclusion of our studies is that the levels of rotation (either diamagnetic or $\mathbf{E} \wedge \mathbf{B}$) present in modern-day tokamaks during Ohmic heating are quite sufficient to make rational magnetic flux surfaces highly resistant to externally induced tearing.

In the linear regime, the response of a rational magnetic surface to an imposed magnetic perturbation of the same helicity is found to be extremely frequency selective. In fact, unless the imposed frequency matches very closely to one of the natural mode frequencies, reconnection at the rational surface is suppressed by a large factor (cf. Sec. II E).

In the nonlinear, regime we predict the suppression of islands propagating with respect to the local equilibrium plasma due to the inertia of the flow pattern set up around them. It is also clear, in addition, that if the island frequency is unable to "lock" onto the imposed frequency, then the induced island size will be substantially reduced. It is convenient to express the strength of the applied perturbation in terms of the (true) width ($W_c = 2\sqrt{2}w_c$) of the induced is-

land in a nonrotating plasma. Both analytic theory (Sec. III L) and numerical simulations (Sec. IV) predict the presence of a fairly clear-cut threshold for W_c [$(W_c)_{\text{crit}}$, say], above which rotational suppression becomes ineffective and the island proceeds to full reconnection [i.e., $W \to W_c$, where $W = 2\sqrt{2}w$ is the (true) induced island width]. For W_c below the threshold the rotational suppression of reconnection is generally quite marked [i.e., $W \ll W_c$]. For the levels of viscosity typically present in modern-day tokamaks the transition from a rotationally suppressed to a fully reconnected island, as W_c is increased, is generally accompanied by a transition from a nonlocked to a locked mode. We can obtain an estimate for $(W_c)_{\text{crit}}$ in the low viscosity limit (i.e., $\zeta_v \ll 1$) using the following expression (cf. Sec. III M):

$$(W_c)_{\text{crit}} \sim 14.6 \left[(f_{\text{MHD}} \tau_H)^{2/3} / (-\Delta_0' r_s)^{1/3} \right] r_s. \quad (180)$$

Here, f_{MHD} is the typical frequency of MHD activity, τ_H the local hydromagnetic time scale, and r_s the radius of the rational surface.

We end this paper by demonstrating how some recent magnetic feedback data from the COMPASS-C[3] device can be interpreted in terms of rotation effects. The typical machine parameters for an Ohmically heated discharge are $a = 20$ cm, $r_s \sim 15$ cm $(m = 2, n = 1)$, $f_{\text{MHD}} \sim 15$ kHz, $\tau_H \sim 10^{-7}$ sec, $\sim 10^6$.

Let us first consider islands induced by stray error fields. In COMPASS-C the $n = 1$ field errors are observed to be $\delta B_\theta / B_\theta \lesssim 5 \times 10^{-4}$. If we assume that say 10% of this field has $m = 2$ poloidal symmetry, then in a *nonrotating* plasma we might expect the field errors to drive a (2,1) island of width $\sim 2\%$ of the minor radius. Note that such an island is significantly wider than the typical (2,1) linear layer width, which is about 0.5% of the minor radius. For the comparatively small islands induced by error fields the rotational suppression factor is of order the linear value calculated in Sec. II E (i.e., a factor of 10 in island size). Thus, in COMPASS-C we would expect the (2, 1) error field island to be rotationally suppressed down to a level where its width is comparable with, or possibly even significantly smaller than, the linear layer width. This is a particularly interesting result, since it implies that the oft-quoted argument that linear theory is invalidated by stray error fields in realistic experimental situations is probably incorrect. In fact, rotation effects ensure that rotational magnetic flux surfaces are highly resistant to tearing induced by field errors. We conclude, therefore, that there is no reason why linear theory should not be employed to predict the *onset* of instability in MHD modes.

In certain low-density COMPASS-C discharges a (2,1) mode saturated at a level $W/a \sim 5\%$ is observed rotating at about 15 kHz. When a stationary (2, 1) magnetic perturbation of appropriate amplitude is applied to the edge of the plasma, via saddle coil external to the vacuum vessel, the frequency of the mode is observed to fall by 2–3 kHz while the amplitude simultaneously decays into the noise.[3] Clearly, 15 kHz is the natural frequency of the (2, 1) mode. We expect an island rotating with this frequency to be stationary with respect to the local equilibrium plasma, and therefore to experience little or no rotational suppression. When the coil current is switched on the island experiences a torque that opposes its rotation. Naturally, the island slows down, but in doing so it has to propagate through the local equilibrium plasma and, therefore, starts to experience a rotational suppression force. It is easily demonstrated that the force associated with a frequency shift of a few kHz is adequate to significantly stabilize a 5% island.

Disruptions may be stimulated in COMPASS-C far from the usual operating boundaries if the current in the saddle coils is sufficiently high. In fact, a disruption almost invariably occurs when the coil current is raised to a level sufficient to induce a 15% (2, 1) island in a nonrotating plasma for $q_{\text{edge}} \lesssim 3$.[3] (This is about twice the current required to stabilize a saturated rotating mode.) Now, our theory predicts that when the coil current exceeds a certain threshold, rotational suppression becomes negligible and the amount of reconnected flux (and therefore the island size) increases markedly. Associated with this sudden increase in the island width is a transformation from a nonlocked to a locked mode. From Eq. (180) we calculate that for a (2, 1) mode in COMPASS-C the threshold occurs when the coil current is capable of driving a $\sim 13\%$ island. It seems quite plausible, then, that the observed disruption limit lies close to or slightly beyond the point at which rotational suppression of the (2, 1) mode is overcome and the island proceeds to full reconnection. Note, however, that the loss of resistive wall stabilization of the mode, due to mode locking, may also play a part in stimulating disruptions.[25,26]

Using our nonlinear theory of propagating magnetic islands, we have been able to present a possible explanation as to why an applied resonant magnetic perturbation sometimes causes mode suppression in COMPASS-C, and sometimes leads to a disruption. We conjecture that the same sort of ideas can be used to explain the much earlier PULSATOR[1] and ATC[27] observations.

In this paper, we have laid the groundwork for the study of the interaction of resonant magnetic perturbations with rotating plasmas, and demonstrated the great relevance of this topic to experiments. Possible extensions of our work might include the solution of the full time-dependent nonlinear problem, and the systematic inclusion of toroidal, resistive wall, and ion diamagnetic effects. It is also vitally important, if any further progress is to be made in this field, to gain a clear understanding of the mechanism that allows Ohmic plasmas to rotate in the absence of any obvious momentum input.

ACKNOWLEDGMENTS

APPENDIX: FLUX-SURFACE AVERAGES

Let

$$\mu = \cos(\xi/2)/k,$$

$$u = \sin^{-1}(\mu),$$
$$v = \cos(\xi/2),$$ \hfill (A1)
$$v = \sin^{-1}(v),$$
$$k = (1/\sqrt{2})(1+\Omega)^{1/2},$$

then

$$X = \sqrt{2}k\cos u,$$
$$\Theta = F(u,k),$$
$$\Xi = \frac{2[E(k)F(u,k) - E(u,k)K(k)]}{K(k)},$$ \hfill (A2)
$$\langle(\cdots)\rangle = \frac{\sqrt{2}}{\pi}\int_0^{\pi/2}\frac{(\cdots)du}{(1 - k^2\sin^2 u)^{1/2}}$$

inside the separatrix ($k < 1$), and

$$X = \sqrt{2}k(1 - k^{-2}\sin^2 v)^{1/2},$$
$$\Xi = \frac{2k[K(1/k)F(v,1/k) - E(v,1/k)K(1/k)]}{K(1/k)},$$ \hfill (A3)
$$\langle(\cdots)\rangle = \frac{\sqrt{2}}{\pi}\frac{1}{k}\int_0^{\pi/2}\frac{(\cdots)dv}{(1 - k^{-2}\sin^2 v)^{1/2}}$$

outside the separatrix ($k > 1$). Beyond the separatrix the analytic continuation of the function Θ (which is no longer periodic in ξ) has the form

$$\Theta = (1/k)F(v,1/k).$$ \hfill (A4)

In the above, E, F, $\mathbf{E}$, and $\mathbf{F}$ are all standard elliptic integrals, and are defined as follows:

$$F(\varphi,l) = \int_0^\varphi \frac{d\alpha}{(1 - l^2\sin^2\alpha)^{1/2}},$$
$$E(\varphi,l) = \int_0^\varphi (1 - l^2\sin^2\alpha)^{1/2}\, d\alpha,$$
$$\mathbf{K}(l) = F(\pi/2,l),$$ \hfill (A5)
$$\mathbf{E}(l) = E(\pi/2,l).$$

Let
$$Z_n(\Omega) \equiv \langle X^n\rangle,$$ \hfill (A6)

then it is easily demonstrated that

$$Z_0(\Omega) = (2/\pi)(1\sqrt{2})\mathbf{K}(k),$$
$$Z_1(\Omega) = (2/\pi)\sin^{-1}(k),$$
$$Z_2(\Omega) = (2/\pi)\sqrt{2}[-(1 - k^2)\mathbf{K}(k) + \mathbf{E}(k)],$$
$$Z_3(\Omega) = (2/\pi)[k(1 - k^2)^{1/2} + (2k^2 - 1)\sin^{-1}(k)],$$ \hfill (A7)
$$Z_4(\Omega) = \frac{2}{\pi}2\sqrt{2}\Big[\Big(k^4 - \frac{5}{3}k^2 + \frac{2}{3}\Big)\mathbf{K}(k)$$
$$+ \frac{2}{3}(2k^2 - 1)\mathbf{E}(k)\Big],$$

$$Z_5(\Omega) = \frac{2}{\pi}\Big[\frac{3}{2}(2k^2 - 1)k(1 - k^2)^{1/2}$$
$$+ 4\Big(k^4 - k^2 + \frac{3}{8}\Big)\sin^{-1}(k)\Big],$$

for $k < 1$, and

$$Z_0(\Omega) = \frac{2}{\pi}\frac{1}{\sqrt{2}}\frac{1}{k}\mathbf{K}\Big(\frac{1}{k}\Big),$$
$$Z_1(\Omega) = 1,$$
$$Z_2(\Omega) = (2/\pi)\sqrt{2}k\,\mathbf{E}(1/k),$$
$$Z_3(\Omega) = (2k^2 - 1),$$ \hfill (A8)
$$Z_4 = \frac{2}{\pi}2\sqrt{2}\Big[-\frac{1}{3}(k^2 - 1)k\,\mathbf{K}\Big(\frac{1}{k}\Big)$$
$$+ \frac{2}{3}(2k^2 - 1)k\,\mathbf{E}\Big(\frac{1}{k}\Big)\Big],$$
$$Z_5(\Omega) = 4\Big(k^4 - k^2 + \frac{3}{8}\Big),$$

for $k > 1$. Note that Z_0 is logarithmically divergent at $k = 1$ (i.e., $\langle 1\rangle$ is logarithmically divergent at the separatrix).

The following flux-surface averages, which are all expressible in terms of the Z_n, are required for the calculation of flow patterns and current distributions around the island:

$$A_0(\Omega) = \frac{\langle X^2\rangle}{\langle 1\rangle} = \frac{Z_2}{Z_0},$$

$$A_1(\Omega) = \frac{\langle X^4\rangle}{\langle 1\rangle} = \frac{Z_4}{Z_0},$$

$$A_2(\Omega) = \frac{\langle\cos\xi\rangle^2}{\langle 1\rangle} = Z_0\Big((2k^2 - 1) - \frac{Z_2}{Z_0}\Big)^2,$$

$$A_3(\Omega) = \langle\Xi X\sin\xi\rangle = \frac{1}{\sqrt{2}}\langle\tilde{X}^2\cos\xi\rangle$$
$$= -\frac{1}{\sqrt{2}}\Big(Z_4 - Z_2\frac{Z_2}{Z_4}\Big),$$ \hfill (A9)
$$A_4(\Omega) = \langle X\tilde{X}^2\rangle = [Z_3 - Z_2(Z_1/Z_0)],$$
$$A_5(\Omega) = \langle X\tilde{X}^4\rangle = [Z_5 - Z_4(Z_1/Z_0)].$$

All of the A_n vary logarithmically in the vicinity of the separatrix, but only A_2 actually diverges. Note that

$$A_0 \to k^2,$$
$$A_1 \to \tfrac{3}{2}k^4,$$ \hfill (A10)

as $k \to 0$. It is also helpful to define the function

$$A_{3'}(\Omega) = \frac{1}{\sqrt{2}}\langle X^2\widetilde{\cos}\xi\,\Theta^2\rangle$$
$$= -\frac{1}{\sqrt{2}}\Big(\langle X^4\Theta^2\rangle - \langle X^2\Theta^2\rangle\frac{Z_2}{Z_0}\Big).$$ \hfill (A11)

The above integral cannot be evaluated analytically throughout the whole of the region $k = [0,1]$. However, in the limit as $k \to 1$ the integral has the limiting form

$$A_{3'} \to -(1/\sqrt{2})(0.3871 - 0.7404A_0) + O(1-k).$$ \hfill (A12)

The determination of the diffusion operators $\breve{\nabla}_1^2$ and $\breve{\nabla}_1^4$

requires the evaluation of the following flux-surface averages:

$$B_0(\Omega) = \frac{\langle \frac{1}{2}\Theta\Theta' + \Theta\Theta'' X^2 \rangle}{\langle 1 \rangle},$$

$$B_1(\Omega) = \frac{\langle \frac{1}{2}\Theta\Theta + 2\Theta\Theta' X^2 \rangle}{\langle 1 \rangle},$$

$$B_2(\Omega) = \frac{\langle \Theta\Theta X^2 \rangle}{\langle 1 \rangle}, \tag{A13}$$

and

$$C_0(\Omega) = \frac{\langle \frac{3}{4}\Theta\Theta'' + 3\Theta\Theta''' X^2 + \Theta\Theta'''' X^4 \rangle}{\langle 1 \rangle},$$

$$C_1(\Omega) = \frac{\langle \frac{3}{2}\Theta\Theta' + 9\Theta\Theta'' X^2 + 4\Theta\Theta''' X^4 \rangle}{\langle 1 \rangle},$$

$$C_2(\Omega) = \frac{\langle \frac{3}{4}\Theta\Theta + 9\Theta\Theta' X^2 + 6\Theta\Theta'' X^4 \rangle}{\langle 1 \rangle}, \tag{A14}$$

$$C_3(\Omega) = \frac{\langle 3\Theta\Theta X^2 + 4\Theta\Theta' X^4 \rangle}{\langle 1 \rangle},$$

$$C_4(\Omega) = \frac{\langle \Theta\Theta X^4 \rangle}{\langle 1 \rangle}.$$

Here, ' denotes

$$\frac{\partial}{\partial \Omega}\bigg|_{\xi} = \frac{1}{2k}\left(\frac{\partial}{\partial k}\bigg|_{u} - \frac{\tan u}{k}\frac{\partial}{\partial u}\bigg|_{k}\right). \tag{A15}$$

Note that B_{0-2} and C_{0-4} are only defined inside the separatrix ($k < 1$). The B_i and the C_i can be evaluated using (A2), (A5), and (A15). It can be shown that

$$C_0 \to -0.0234/k^4,$$
$$C_1 \to 0.1250/k^2,$$
$$C_2 \to 0.1481, \tag{A16}$$
$$C_3 \to 0.5924k^2,$$
$$C_4 \to 0.2962k^4,$$

as $k \to 0$. In the limit as $k \to 1$, the functions B_0 and C_1 diverge like $1/(1-k)$, while C_0 diverges like $1(1-k)^2$. This divergent behavior emanates from a region around $X = 0$ of angular extent (in ξ) $(1-k^2)^{1/2}$.

Finally, the determination of the current profiles around the island requires the evaluation of the following flux-surface averages:

$$D_0(\Omega) = \left\langle \Xi\left(-\frac{1}{2}\frac{1}{\sqrt{2}}\frac{\Theta'}{X^2} + \frac{3}{2}\frac{1}{\sqrt{2}}\Theta'' \right.\right.$$
$$\left.\left. + \frac{1}{\sqrt{2}}X^2\Theta''' + X\sin\xi\,\Theta'\Theta'' \right)\right\rangle,$$

$$D_1(\Omega) = \left\langle \Xi\left(-\frac{1}{2}\frac{1}{\sqrt{2}}\frac{\Theta}{X^2} + X\sin\xi\,\Theta\Theta'' \right.\right.$$
$$\left.\left. + \frac{7}{2}\frac{1}{\sqrt{2}}\Theta' + \frac{3}{\sqrt{2}}X^2\Theta'' + 2\sin\xi\,\Theta'\Theta' \right)\right\rangle,$$

$$D_2(\Omega) = \left\langle \Xi\left(\frac{3}{2}\frac{1}{\sqrt{2}}\Theta + \frac{2}{\sqrt{2}}X^2\Theta' + X\sin\xi\,\Theta\Theta' \right)\right\rangle, \tag{A17}$$

$$D_3(\Omega) = \left\langle \Xi\left(\frac{1}{2}\frac{1}{\sqrt{2}}\Theta + 2X\sin\xi\,\Theta\Theta' \right)\right\rangle,$$

$$D_4(\Omega) = \left\langle \Xi\left(\frac{1}{\sqrt{2}}X^2\Theta \right)\right\rangle,$$

$$D_5(\Omega) = \left\langle \Xi\left(-\frac{1}{\sqrt{2}}X^2\Theta + X\sin\xi\,\Theta\Theta \right)\right\rangle,$$

and

$$E_0(\Omega) = \left\langle X\left(-\frac{1}{2}\frac{1}{\sqrt{2}}\frac{1}{X^2} + X\sin\xi\,\Theta'' \right)\right\rangle,$$

$$E_1(\Omega) = \left\langle X\left(\frac{3}{2}\frac{1}{\sqrt{2}} + X\sin\xi\,\Theta' \right)\right\rangle,$$

$$E_2(\Omega) = \left\langle X\left(\frac{1}{2}\frac{1}{\sqrt{2}} + 2X\sin\xi\,\Theta' \right)\right\rangle,$$

$$E_3(\Omega) = \left\langle X\left(-\frac{1}{\sqrt{2}}X^2 + X\sin\xi\,\Theta \right)\right\rangle, \tag{A18}$$

$$E_4(\Omega) = \left\langle X\left(\frac{1}{\sqrt{2}}X^2 \right)\right\rangle,$$

$$E_5(\Omega) = \langle X(X\sin\xi\,\Theta) \rangle.$$

Note that D_{1-5} and E_{1-5} are only defined in the region $k < 1$. The D_i and E_i can be evaluated using (A2), (A5), and (A15).

[1] F. Karger, H. Wobig, S. Corti, J. Gernhardt, O. Klüber, G. Lisitano, K. McCormick, D. Meisel, and S. Sesnic, in *Plasma Physics and Controlled Nuclear Fusion Research 1974*, Proceedings of the 5th International Conference, Tokyo (IAEA, Vienna, 1975), Vol. 1, p. 207.

[2] J. J. Ellis, A. A. Howling, A. W. Morris, and D. C. Robinson, in *Plasma Physics and Controlled Nuclear Fusion Research 1984*, Proceedings of the 10th International Conference, London (IAEA, Vienna, 1985), Vol. 1, p. 363.

[3] A. W. Morris, R. Fitzpatrick, P. S. Haynes, T. C. Hender, J. Hugill, C. Silvester, and T. N. Todd, in *Controlled Fusion and Plasma Heating 1990*, Proceedings of the 17th European Conference, Amsterdam (EPS, Geneva, 1990), Vol. 1, p. 379.

[4] J. A. Snipes, D. J. Campbell, P. S. Haynes, T. C. Hender, M. Hugon, P. J. Lomas, N. J. Lopus Cardozo, M. F. F. Nave, and F. C. Schüller, Nucl. Fusion 28, 1085 (1988).

[5] J. W. Connor, S. C. Cowley, R. J. Hastie, T. C. Hender, A. Hood, and T. S. Martin, Phys. Fluids 31, 577 (1988).

[6] S. C. Cowley and R. J. Hastie, Phys. Fluids 31, 426 (1988).

[7] R. B. White, D. A. Monticello, M. N. Rosenbluth, and B. V. Waddell, Phys. Fluids 20, 800 (1977).

[8] T. S. Hahm and R. M. Kulsrud, Phys. Fluids 28, 2412 (1985).

[9] M. F. F. Nave and J. A. Wesson, in *Controlled Fusion and Plasma Physics 1987*, Proceedings of the 14th European Conference, Madrid (EPS, Geneva, 1987), Vol. 3, p. 1103.

[10] H. P. Furth, J. Killeen, and M. N. Rosenbluth, Phys. Fluids 6, 459 (1963).

[11] H. H. Glasser, J. M. Greene, and J. L. Johnson, Phys. Fluids 18, 875 (1975).

[12] G. Ara, B. Basu, B. Coppi, G. Laval, M. N. Rosenbluth, and B. V. Waddell, Ann. Phys. (NY) 112, 443 (1978).

[13] J. F. Drake and Y. C. Lee, Phys. Fluids 20, 1341 (1977).

[14] D. Stork, A. Boileau, F. Bombarda, D. J. Campbell, C. Challis, W. G. Core, B. Denne, P. Duperrex, R. Giannella, L. Horten, T. T. C. Jones, E. Källne, A. Pochelon, J. Ramette, B. Saoutic, D. Schram, J. Snipes, G. Tallents, E. Thompson, G. Tonetti, M. von Hellerman, and J. Wesson, in Ref. 9, Vol. 1, p. 306.

[15] A. Bondeson and R. Iacono, in *Theory of Fusion Plasmas*, Proceedings of the Joint Varrenna-Lausanne International Workshop, Chexbres 1988

672   Phys. Fluids B, Vol. 3, No. 3, March 1991

R. Fitzpatrick and T. C. Hender   672

(SIF, Bologna, 1989), p. 57.

[16] P. H. Rutherford, Phys. Fluids **16**, 1903 (1973).

[17] D. Edery, M. Frey, J. P. Somon, M. Tagger, J. L. Soule, R. Pellat, and M. N. Bussac, Phys. Fluids **26**, 1165 (1983).

[18] S. I. Braginskii, in *Reviews of Plasma Physics*, edited by M. A. Leontovich (Consultants Bureau, New York, 1965), Vol. 1, p. 205.

[19] B. D. Scott and A. B. Hassam, Phys. Fluids **30**, 90 (1987).

[20] D. Biskamp, Nucl. Fusion **18**, 1059 (1978).

[21] B. D. Scott, A. B. Hassam, and J. F. Drake, Phys. Fluids **28**, 275 (1985).

[22] E. Lazzaro and M. F. F. Nave, Phys. Fluids **31**, 1623 (1988).

[23] H. R. Strauss, Phys. Fluids **19**, 134 (1976).

[24] H. R. Hicks, B. A. Carreras, J. A. Holmes, D. K. Lee, and B. V. Waddell, J. Comp. Phys. **44**, 46 (1981).

[25] T. C. Hender, C. G. Gimblett, and D. C. Robinson, Nucl. Fusion **29**, 1279 (1989).

[26] M. Persson and A. Bondeson, Nucl. Fusion **29**, 989 (1989).

[27] K. Bol, J. L. Cecchi, C. C. Daughney, F. DeMarco, R. A. Ellis, H. P. Eubank, H. P. Furth, H. Hsuan, E. Mazzucato, and R. R. Smith, in Ref. 1, Vol. 1, p. 88.

.